Technical Report

TR-99-32

Creep in buffer clay

Roland Pusch
Geodevelopment AB

Robert Adey
Computational Mechanics BEASY

December 1999

Svensk Kärnbränslehantering AB
Swedish Nuclear Fuel
and Waste Management Co
Box 5864
SE-102 40 Stockholm Sweden
Tel 08-459 84 00
+46 8 459 84 00
Fax 08-661 57 19
+46 8 661 57 19

Creep in buffer clay

Roland Pusch

Geodevelopment AB

Robert Adey

Computational Mechanics BEASY

December 1999

ABSTRACT

The number of particles and wide range of the particle bond spectrum in the buffer clay require use of stochastical mechanics and thermodynamics for adequate modeling of creep and they are basic to the model proposed for predicting creep settlement. The predicted shear-induced creep settlement under constant volume conditions using the model is on the order of 1 mm in ten thousand years and up to a couple of millimeters in one million years and much smaller than the consolidation settlement, which may be about 10 mm. The general conclusion is that creep settlement of the canisters is very small and of no significance to the integrity of the buffer itself or of the canisters.

LIST OF CONTENTS

		Page
1	INTRODUCTION	5
2	CONSTITUTION OF MX-80 CLAY	6
2.1	Mineral components, clay particles	6
2.2	Clay particle aggregates	6
2.3	Evolution of microstructure	7
2.3.1	Introduction	7
2.3.2	Crystal structure of montmorillonite	8
2.3.3	Constitution of smectite stacks of MX-80 clay	8
2.3.4	Constitution of grains containing aggregates of smectite stacks	9
2.3.5	Primary structure of blocks of compacted MX-80 powder	10
2.3.6	Structure of blocks of compacted MX-80 powder after hydration	11
2.3.7	Microstructural variations in blocks of compacted, hydrated blocks	14
3	INTERPARTICLE BONDS IN SMECTITE CLAY	19
3.1	Particle contacts	19
3.2	Physical state and properties of porewater	20
3.3	Evaluation of interparticle bonds	20
3.4	Interparticle bond spectrum	23
4	COMMON CREEP MODELS	24
4.1	Introduction	24
4.2	Mathematical form of current creep models	25
4.2.1	General	26
4.2.2	The stress parameter D	26
4.2.3	The time parameter n	27
4.2.4	Criteria for a creep model for predicting canister settlement	28
5	CREEP MODEL PROPOSED FOR PREDICTING CANISTER SETTLEMENT	29
5.1	Introduction	29
5.2	The stochastic model	30
5.2.1	Basic features	31
5.2.2	General performance of the model	32
5.2.3	Influence of stress	33
5.2.4	Influence of temperature	34
5.2.5	Influence of porewater chemistry	35
5.2.6	Influence of mineral changes	36
5.2.7	General comments	37
6	PREDICTION OF CANISTER SETTLEMENT	39
6.1	Background	39
6.2	Laboratory-scale experiments	39
6.3	Field experiment	43
6.4	Prediction of canister settlement	43
7	DISCUSSION AND CONCLUSIONS	46
8	REFERENCES	51
9	APPENDIX	54

SAMMANFATTNING

Undersökningen omfattade karakterisering av den mikrostrukturella uppbyggnaden och kraftfälten på molekylär nivå i buffertleran för att få en grund för val av lämpliga krypmodeller. Slutsatsen är att den stora mängden partiklar och breda spektrum för partikelbindningarna kräver att stokastisk mekanik och termodynamik beaktas. Det är fallet med den föreslagna modellen för prediktering av krypbetingad sättning hos kapslarna.

Inverkan av spänningsnivån på krypdeformationerna hos MX-80 lera är inte väl känd men för buffertleran gäller approximativt proportionalitet mellan spänning och krypning. Teoretiskt sett är temperaturens inverkan liten för temperaturer upp till 90°C och det stöds av modellexperiment och approximativt gäller proportionalitet mellan temperatur och krypning för bufferten. Den allmänna funktionen hos den stokastiska modellen kan i princip åskådliggöras med hjälp av viskoelastiska modeller med en tidsberoende ökning av viskositeten.

Den beräknade skjuvningsinducerade krypsättningen är ca 1 mm på tiotusen år och upp till ett par millimeter på en miljon år. Den allmänna slutsatsen är att krypsättningen hos kapslarna är mycket liten och av försumbar betydelse för buffertens och kapslarnas tillstånd.

SUMMARY

The study involved characterization of the microstructural arrangement and molecular force-fields in the buffer clay for getting a basis for selecting suitable creep models. It is concluded that the number of particles and wide range of the particle bond spectrum require that stochastical mechanics and thermodynamics be considered and they are basic to the creep model proposed for predicting creep settlement of the canisters.

The influence of the stress level on creep strain of MX-80 clay is not well known but for the buffer creep is approximately proportional to stress. Theoretical considerations suggest a moderate impact for temperatures up to 90°C and this is supported by model experiments. It is believed that the assumption of strain being proportional to temperature is conservative. The general performance of the stochastic model can be illustrated in principle by use of visco-elastic rheological models implying a time-related increase in viscosity.

The shear-induced creep settlement under constant volume conditions calculated by using the proposed creep model is on the order of 1 mm in ten thousand years and up to a couple of millimeters in one million years. It is much smaller than the consolidation settlement, which is believed to be on the order of 10 mm. The general conclusion is that creep settlement of the canisters is very small and of no significance to the integrity of the buffer itself or of the canisters.

1 INTRODUCTION

Creep, i.e. time-dependent strain, under drained or undrained conditions will take place in the canister-embedding clay due to the load exerted by the heavy canisters and make them settle. The creep, which is caused by compression (consolidation) and shear deformation of the clay, is of practical importance since it may bring the canisters down to the bottom of the deposition holes leaving no buffering clay between the canisters and the rock.

The strain history will in fact be complex since the movement of the canisters is affected by variations in density and different rates of wetting of different parts of the buffer, a major process being upheaval of the canisters in the first few years due to upward expansion of the buffer in conjunction with compression of the overlying tunnel backfill. Since the initial upward canister movement will not cause any problem, while long-term settlement may be critical, the present study will deal only with the downward canister movement that takes place after several years. A number of simplifications will be made:

1. The development of theories for description and prediction of canister settlement will be based on the assumption that the canisters are applied instantly in the buffer clay.

2. The buffer clay is assumed to be fully water saturated and homogeneous, i.e. with only statistically distributed density variations on the microscale.

3. The buffer is assumed to be confined by the rock and the overlying backfill without any yield of these boundaries.

2 CONSTITUTION OF MX-80 CLAY

2.1 Mineral components, clay particles

The size of montmorillonite particles in MX-80 clay is illustrated by Figure 1, which shows the distribution of the maximum diameter (crystallographic a/b plane) of stable stacks of lamellae [1]. One finds that about 5 % of the particles are smaller than 0.1 μm while 40 % of the particles are smaller than 0.15 μm. This latter fraction, which is taken to be truly colloidal with some approximation, has a specific surface area of at least 2000 m^2 per gram solid mineral mass and hence represents the most surface-active part of MX-80 clay.

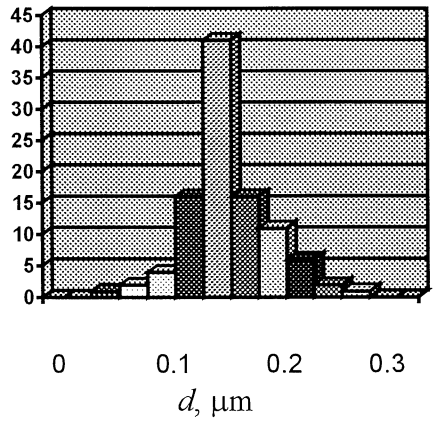

Figure 1. *Frequency (vertical axis) of maximum diameter d of small particles of effectively dispersed Na montmorillonite as evaluated by transmission electron microscopy [1]. 0.1 μm=100 nm.*

2.2 Clay particle aggregates

MX-80 bentonite clay is produced by the company American Colloid Co through drying and grinding bentonite material that is scraped off layer-wise from the ground. This yields granulated powder with a water content of around 10 % (mass of water given off at 105°C, divided by mass of solid remainder). The size distribution of the granules, which contain billions of stacks of lamellae, is illustrated in Figure 2.

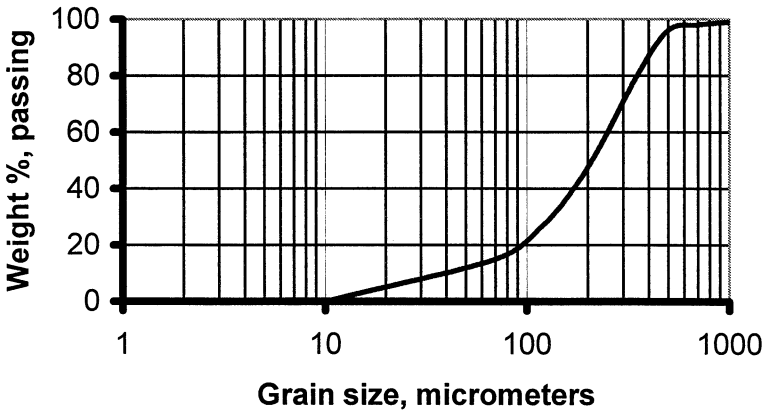

Figure 2. *Size distribution of MX-80 grains (granules) [2].*

2.3 Evolution of clay microstructure

2.3.1 Introduction

The arrangement of smectite particles and the distance and forces between them determine the swelling pressure, the rheological behavior and how much water that is mobile under ordinary hydraulic gradients. It is hence of basic importance to the present problem.

The following terms are used for the various microstructural constituents:

Flake, lamella: Single sheet of smectite crystal lattice.
Stack of flakes: Coherent particle consisting of a number of aligned lamellae.
Aggregate: Coherent group of stacks.
Clay gel: Coherent porous network of aggregates.
External voids: Air- or water-filled space between stacks of lamellae.
Internal voids: Interlamellar space

Microstructural modelling requires that the composition of the clay material is defined with respect to the size distribution of the powder grains, the amount of smectite and accessory minerals, and the type of adsorbed cations [3]. Bulk MX-80 contains 65-75 % montmorillonite, 10-14 % quartz, 5-9 % feldspars, 2-4 % mica and chlorite, 3-5 % carbonates and chlorite, and 1-3 % heavy minerals. The dominant adsorbed cation is Na (60 %), while Ca represents about 25 % and Mg around 10 %. For simplifying the

microstructural modelling it is assumed that montmorillonite makes up 100 % of the minerals. The derived models will therefore deviate somewhat from the true microstructural constitution but this of no concern in the present context.

2.3.2 Crystal structure of montmorillonite

Definition of the crystal structure of montmorillonite requires that a stack of at least two lamellae of the type shown in Figure 3 are considered [2,3]. Both models are theoretically possible, the traditional Hofmann/Endell/Wilm version being valid for elevated temperature and adsorption of other cations than Li and Na, while the Edelman/Favejee version may apply to lower temperatures than about 100°C with Li and Na in exchange positions. The latter model implies that more OH-radicals are available than in the firstmentioned model, in which OH is exposed only at the particle edges. The models hence imply different interparticle forces, which has to be considered in the present context.

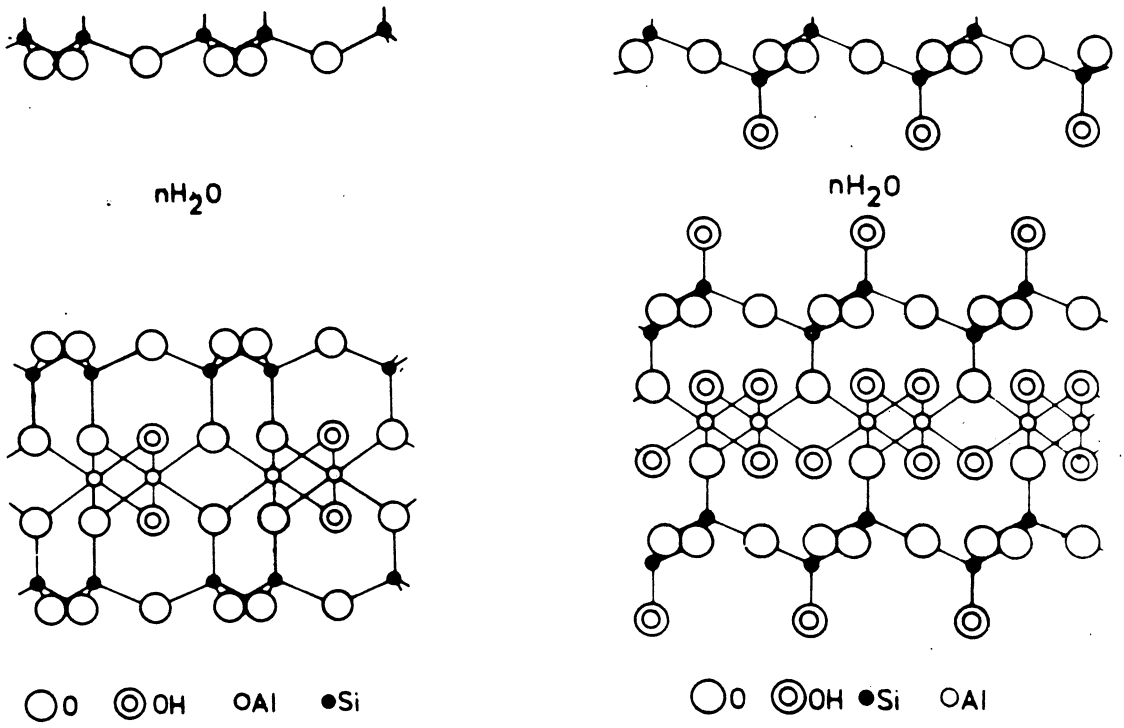

Figure 3. Montmorillonite structure. Left: Hofmann/Endell/Wilm. Right: Edelman/Favejee [2,3].

2.3.3 Constitution of smectite stacks of MX-80 clay

Most of the smectite stacks in air-dry MX-80 stored at 50-70 % RH, have 1 interlamellar hydrate layer but where Ca and Mg are sorbed there are 2 hydrate

layers. When the clay powder is exposed to moist air with RH=100 % or to liquid water, the number of interlamellar hydrate layers increases to maximum 3 when Na is sorbed, while it remains to be 2 when Ca and Mg are sorbed. Table 1 gives estimated basal spacings and average number of interlamellar hydrates for different bulk density intervals.

Table 1. *Interlamellar hydrates in MX-80 clay at water saturation [2].*

Bulk density at saturation, kg/m^3	**Basal spacing, Å**	**Average number of interlamellar hydrates**
2100-2200	13.7-14.6	1
2000-2100	14.6-16.5	1-2
1900-2000	16.5-18.3	2
1700-1900	18.3-19.3	2-3
1500-1700	19.3-23.0	3
1400-1500	23.0-27.0	3*

* Maximum number of interlamellar hydrates of stacks; higher basal spacings indicate the presence of more than one stack

2.3.4 Constitution of grains cointaining aggregates of smectite stacks

The internal structure of MX-80 bentonite grains is inhereted from that of the natural bentonite beds and is therefore usually characterized by more or less aligned aggregates of stacks, which makes the grains anisotropic. This means that the orientation of the grains affects the behavior of the clay in bulk. This is obvious from Figure 4, which illustrates various arrangements of anisotropic grains. It is clear that if all grains are oriented in the same fashion the clay behaves quite differently than if they are randomly oriented.

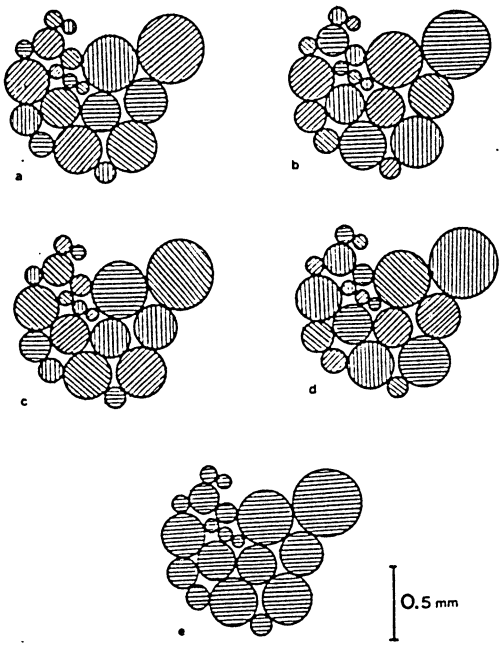

Figure 4. *Orientation patterns of internally anisotropic MX-80 grains.*

2.3.5 Primary structure of blocks of compacted MX-80 powder

According to a method for buffer block production first used by SKB and later considered and applied by POSIVA and ENRESA, air-dry clay powder is poured in a form and compacted uniaxially or triaxially under high pressure to yield highly compacted blocks. For preparation of KBS-3 buffer the clay blocks are manufactured by compacting the powder under a pressure of 100 MPa. The dry density of the grains is about 1980 kg/m^3 for 10 % water content by weight and the dry density of the powder mass poured in the form is about 1200 kg/m^3. Uniaxial compression causes a reduction in void space between the grains and deformation of the grains that has been calculated by applying the boundary element code BEASY [2] assuming the powder grains to behave elastically.

The compressive strain was calculated in 3D taking the initial powder particles to be spherical and to make up a unit cell consisting of one big grain and 8 small grains as illustrated in Figure 5. The diameter 0.35 mm of the big grain and 0.10 mm of the small one yield approximately the grain size distribution in Figure 2. The initial void ratio was 1.08 and the initial "effective" porosity 47 %, both being representative of MX-80 powder before compaction. The resulting reduction in "external" pore volume was 34 % yielding the net dry density 1850 kg/m^3 of the model clay and the density 2050 kg/m^3 after complete water saturation. This is the buffer density that will be focused on in this report.

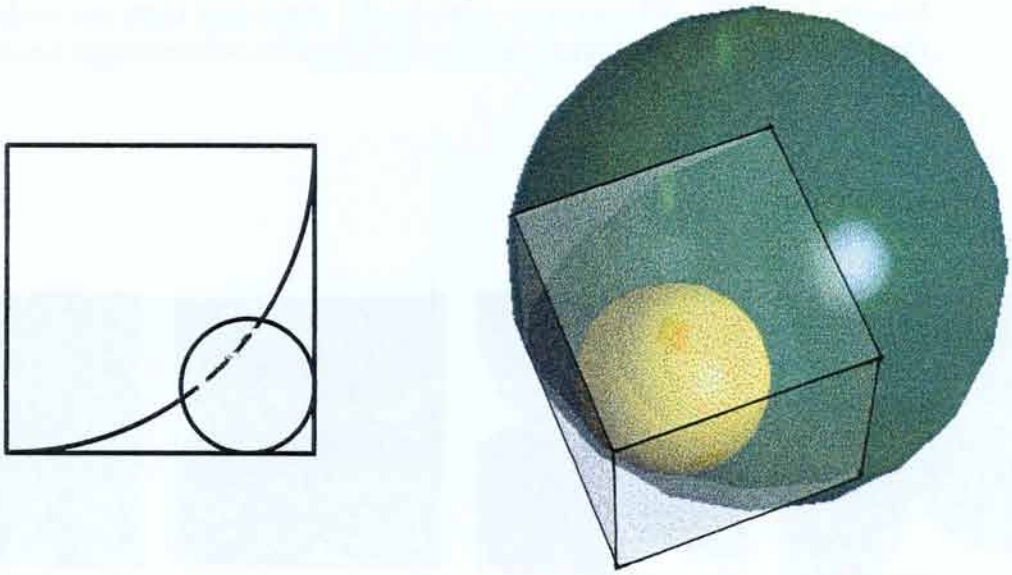

Figure 5. *Unit cell with one eighth of a 0.35 mm diameter grain and one complete 0.10 mm diameter grain.*

2.3.6 Structure of blocks of compacted MX-80 powder after hydration

The initially air-dry clay absorbs water molecules when exposed to vapor or water migrating from the rock. The densest parts of the compressed grains have the highest hydration potential and become wetted quickly if the grains are free to expand, but the hydration is resisted if there is an external pressure or confinement. The rate of water uptake is controlled by the capacity of the clay matrix to provide water, which means that its hydraulic conductivity is a controlling factor.

The grain growth has been simulated by applying the BEASY code using the unit cell model in compressed form [2]. Figure 6 shows a section through the hydrated unit cell oriented perpendicular to the compaction direction at the block manufacturing. There are open voids in all sections and in the tightest ones the open space consists of thre channels with 10-20 μm diameter. In the most open sections there are channels with even larger widths.

While there are no straight open channels between the expanded grains in the clay matrix, there are tortuous paths formed by interconnected voids with a

diameter of down to 10 μm. The statistical distribution of the grain orientation and the fact that the grains do not make up perfect stacks of smectite lamellae but contain small voids between small stacks, mean that there are voids ranging from tens of Å to tens of micrometers including also isolated larger voids.

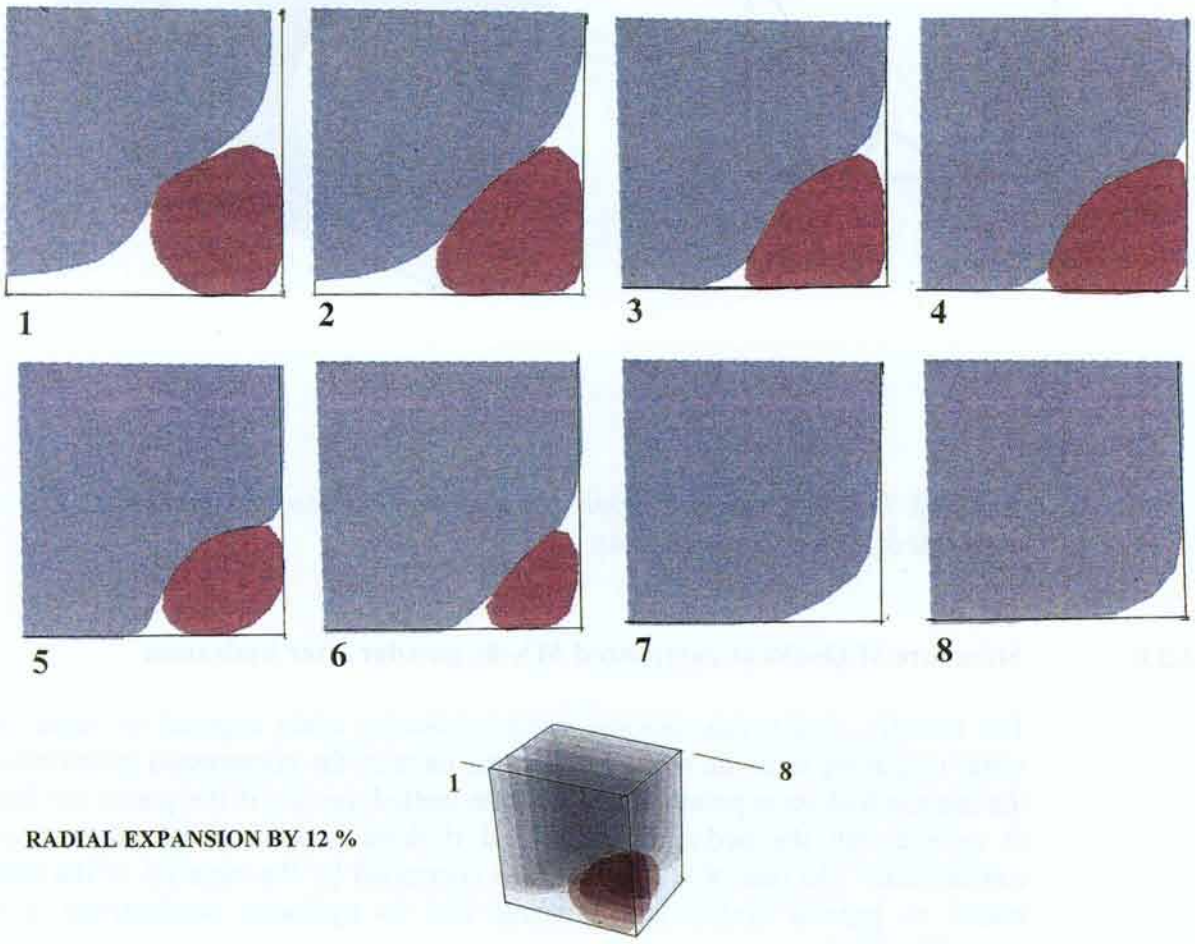

***Figure** 6. Shape of the grains compacted under 100 MPa pressure and subsequently expanded. Calculation by use of BEASY. The eight sections are oriented perpendicularly to the direction of compaction.*

The voids are largely or completely occupied by clay gels formed by exfoliated, dispersed and reorganized smectite particles when Na or Li are in exchange positions. For smectite clay saturated with Ca and Mg the gel-forming capacity is much lower as manifested by the much higher bulk hydraulic conductivity [2].

The voids are largely or completely occupied by clay gels formed by exfoliated, dispersed and reorganized smectite particles when Na or Li are in exchange positions. For smectite clay saturated with Ca and Mg the gel-forming capacity is much lower as manifested by the much higher bulk hydraulic conductivity [2]. The gels are built up of aggregates of colloidal clay particles by coagulation of discrete stacks of lamellae or small groups of stacks released from the dense grains, or they represent particles released as such from the dense grains. In the first case the aggregates result from successive agglomeration of particles, while in the latter case they originate from successive expansion and disintegration of initially denser clay. The size and strength of either aggregate type may not be the same.

Dispersed particles move by Brownian molecular motion and easily form gels if the charge is favorable. The motion is both rotational and translatory, which makes it highly probable that particle contacts are established edge-to-edge [4]. However, the charge distribution over the particle surfaces and also the conditions for bringing particles in close contact affect the way in which adjacent particles make and remain in contact.

The most simple structure model implies that coagulation of dispersed particles takes place by Coulomb-type attraction of nearby particles, i.e. through bonding of the positively charged part of one particle and negatively charged parts of an adjacent particle. There is strong evidence that the edges of the stacks are positively charged in the neutral and weakly alkaline pH range (pH <7-8), cf. Figure 7, while the basal planes carry a negative charge, hence yielding edge-to-face aggregation.The positive charges are believed to result from processes of the type indicated by Eq.1 [5].

Al-O-Al ---> (Al-O + Al) + (H OH) ---> Al-(OH) (1)

Negative edge charge is commonly believed to result from dissociation of structural OH although this is a questionable process since the hydroxyls are bound to lattice aluminum or magnesium and should stay in the lattice, probably in protonated form [5]. Spontaneously approaching particles with negative edge charge and negatively charged basal planes, which conditions prevail at pH>8, can become bonded together by ion-pairing [6].

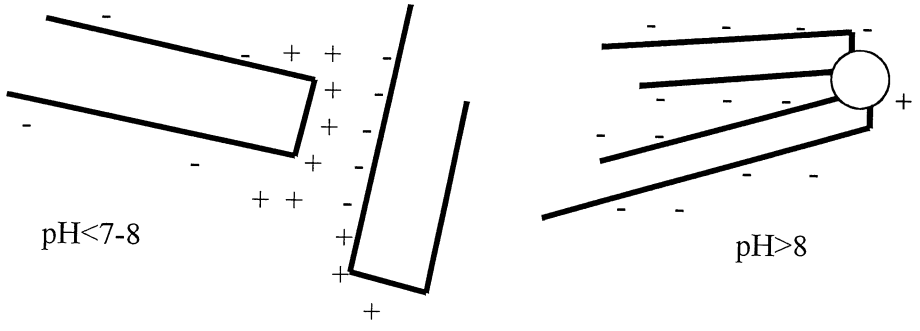

***Figure** 7. Edge charge conditions as a function of pH in the porewater [5].*

Smectite clay particles with the same surface charge in suspensions can also associate in a face-to face fashion by electrical double layer interaction [6]. The coupling is weak, however, except at low and moderate electrolyte contents. Such association may take place spontaneously in suspensions but it commonly emerges from compressed ("consolidated") or sheared states.

In the course of face-to-face coupling, lateral growth of stacks of lamellae may lead to large, i.e. micrometer-sized, flat aggregates. Light scattering and viscosity measurements of montmorillonite gels in the pH range 6-13 have been interpreted as ribbons of edge-to-edge flocs, but cardhouse-type edge-to-face association may also be formed [6]. The latter is believed to dominate at neutral and acid pH.

2.3.7 Microstructural variations in blocks of compacted, hydrated blocks

General

The expansion of the initially air-dry clay powder grains and the formation and consolidation of clay gels in the voids between them lead to varying densities in different parts of the clay. This can be illustrated by examining transmission electron micrographs (TEM) of ultrathin sections of clay specimens prepared by replacement of porewater by suitable resins [7]. Figure 8 illustrates the characteristic microstructure of MX-80 clay with a bulk density at saturation of about 2000 kg/m^3 with dense clay aggregates separated by a less dense clay matrix and local voids in agreement with the numerically deduced microstructural model.

The density variations have been made obvious by digitalizing the micrograph, which also makes it possible to determine the density distribution by integration of scanned areas of different density. Digitalized micrographs can be converted into different colors for easy interpretation and representation of the variation in density. In the current R&D work this is made by transforming scanned micrographs to digitalized form using the OFOTO 2 code, with subsequent coloring using the GRAPHIC CONVERTER 2.9.1 code on a MacIntosh Power PC6100/66 [2]. Using only four colors, clear distinction can be made of parts representing different densities: black parts, i.e. the most electron-absorbing components being the densest parts of the clay matrix, and red parts representing relatively dense parts of the matrix. Green are rather soft, porous gels while white represent very porous gels or open voids.

The dominant interparticle bonds depend on the clay matrix density as laborated on later in the report and since strain is controlled by the bond strength, the density distribution has a major influence on the rheological behavior of the buffer clay.

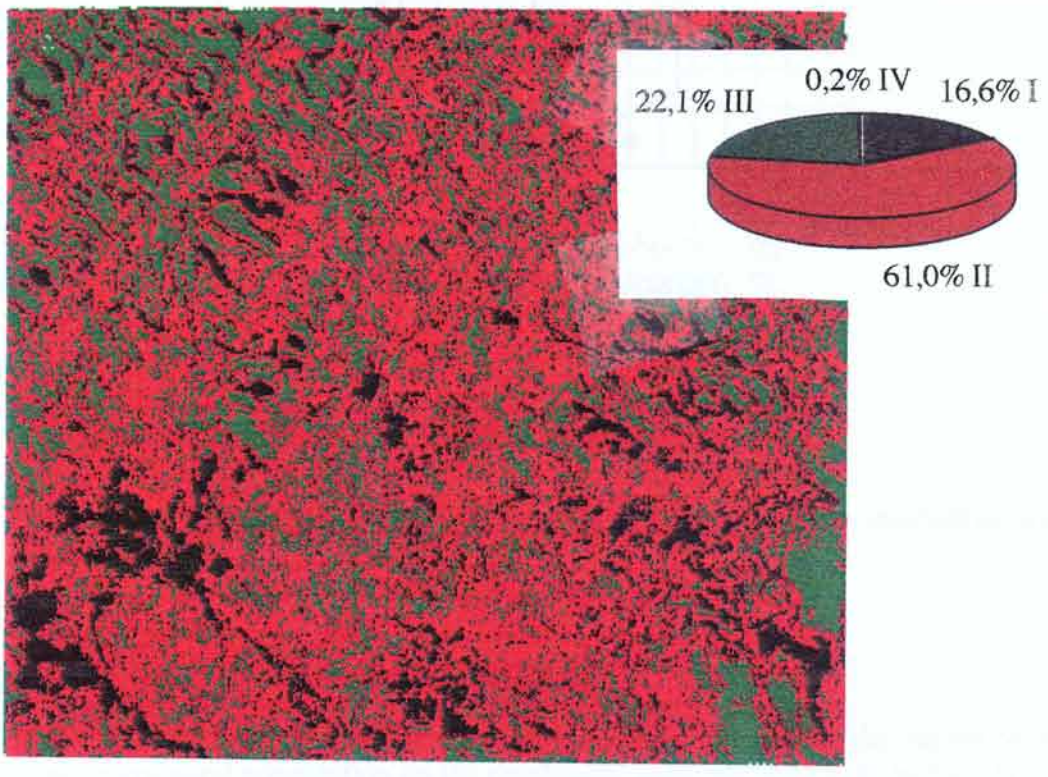

Figure 8. *Transmission electron micrograph of MX-80 clay with a bulk density of 2000 kg/m^3 [2]. The micrograph has been digitalized to make density variations obvious: Black: Most dense parts (density exceeding 2000 kg/m^3), Red: Second densiest parts (about 2000 kg/m^3), Green: Medium dense parts (1500-2000 kg/m^3), and White: Soft gels or open voids (<1500 kg/m^3).*

Microstructural parameters

The clay matrix is defined here to consist of two major components:

1. Stacks, stack aggregates (*a*)
2. Gel-filled voids and unfilled voids (*b*)

This distinction is made on the ground that the firstmentioned components are dense and characterized by other types of interparticle bonds than the gels and that the *a*-components are completely or largely impermeable while the *b* components offer no or little flow resistance. They are related through the coefficients F_2 for 2D and F_3 for 3D conditions as specified in Figure 9 [2].

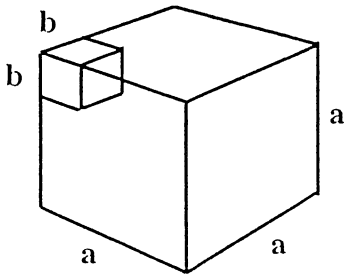

2D $F_2=b^2/a^2$ $b=a(F_2)^{1/2}$

3D $F_3=b^3/a^3$ $F_3=F_2x(F_2)^{1/2}=(F_2)^{3/2}$ $\rho_{av}=\rho_b F_3 + \rho_a(1-F_3)$

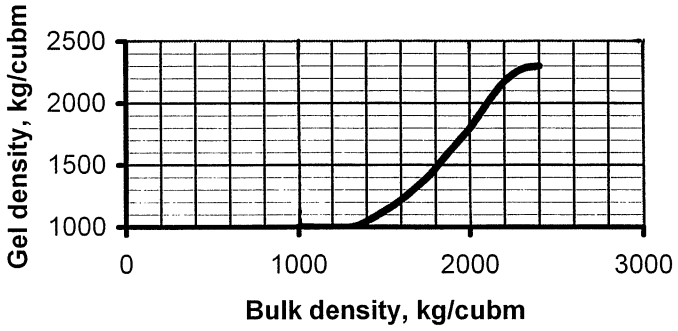

Figure 9. *Microstructural parameters. ρ_{av} is the average bulk density of the clay and ρ_a and ρ_b the average density of components a (stacks, stack aggregates and non-smectitic minerals) and b (soft gel fillings and open space). The diagram shows average gel density (ρ_b) versus average bulk density (ρ_{av}).*

F_2 and F_3 can be evaluated from digitalized TEM micrographs with an edge length of at least 30 μm in order to be representative for the larger part of the clay matrix. One gets the approximate relationship between the average bulk density and the gel density (phase *b* in Figure 9). The *F*-parameters are related to the average bulk density of saturated MX-80 clay as shown in Figure 10 [2]. The relationships can be expressed analytically as well [2].

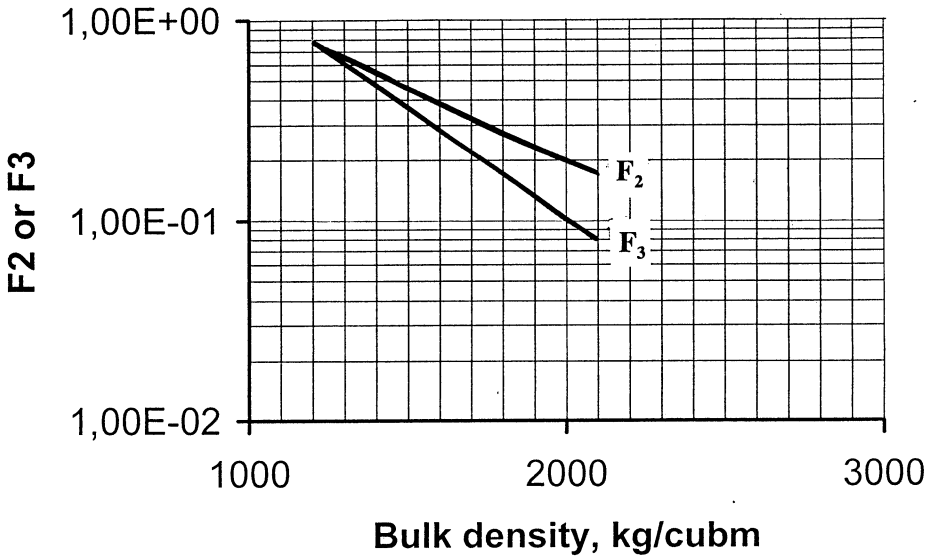

Figure 10. *F_2 and F_3 versus bulk density. Data based on microstructural analysis of MX-80 clay [2].*

Example of relevance of microstructural parameters in rheology

We will take here the bulk swelling pressure as an example of the impact of the microstructural constitution on the rheological behavior of MX-80 buffer clay. It is roughly proportional to the product of the true swelling pressure of the pressure-controlling component *a* and the volume ratio $(a^3\text{-}b^3)/a^3$. This ratio is $(1\text{-}F_3)$, which specifies the volume fraction of this component. For the bulk density 2130 kg/m^3 (ρ_a) is 2150 kg m^3 and the true swelling pressure of this component calculated by use of the Yong/Warkentin theory [8,9] about 11 MPa.

Assuming isotropic distribution of the orientation of the stacks of smectite lamellae F_3 is 0.93 and the product consequently about 10 MPa, which is on the same order of magnitude as the experimentally determined swelling pressure. Theoretical values derived in this fashion for a number of densities are in good agreement with experimental data as illustrated by Table 2, except for rather soft MX-clay in Ca-form. This discrepancy is due to insufficient sensitivity of the model for densities representing conditions close to complete expansion of the densest part of the clay matrix (*a*).

Table 2. *Calculated and experimentally determined swelling pressures (p_s) of MX-80 for Na and Ca saturation.[2].*

Bulk density, kg/m^3	**1-F_3**	**Density of massive part *(a)*, kg/m^3**	**p_s of massive part *(a)* MPa**	**Calculated bulk p_s MPa**	**Experiment-al bulk p_s MPa**
Distilled water					
2130 Na	0.93	2150	11	10	10-15
1850 Na	0.80	1900	1.5	1.2	1.0
1570 Na	0.75	1750	0.3	0.2	0.3
3.5 % $CaCl_2$ solution					
2130 Ca	0.93	2150	11	10	10-15
1850 Ca	0.80	1900	1.5	1.2	1.0
1570 Ca	0.75	1750	0.3	0.2	0.02

As to the influence of increased salinity with Na as dominant cation in the porewater of MX-80 clay with a bulk density 2130 kg/m^3, the swelling pressure is the same as for saturation with distilled water, while for 1850 kg/m^3 the theoretical value is around 1.0 MPa and a typical experimental value about 0.5 MPa. For the lowest bulk density 1570 kg/m^3 the theoretical swelling pressure is about 0.15 MPa, while recorded swelling pressures are only a few tens of kPa. Hence, in general, the theoretical model overestimates the swelling pressure of soft MX-80 clay with electrolyte-rich porewater.

The general conclusion from the examination of the relationship between the microstructural parameters and the swelling pressure is that the theoretical model applies in principle. For a buffer clay density of about 2050 kg/m^3 it is believed that (1-F_3) is about 0.90, meaning that 90 % of the volume of a clay unit consists of aggregates of stacks of lamellae with an average density of around 2100 kg/m^3, yielding a net bulk swelling pressure of about 7 MPa.

3 INTERPARTICLE BONDS IN SMECTITE CLAY

3.1 Particle contacts

Figure 11 illustrates the various types of contacts and discontinuities on the microstructural scale. While the large majority of the clay particles in dense aggregates of matured MX-80 clay consist of stacks of equally oriented 10 Å lamellae separated by water molecules and cations, the softer gels may imply edge-to-edge, face-to-face, and edge-to face coupling. This means that different types of bonds between the mineral constituents are expected and that there is a bond strength spectrum.

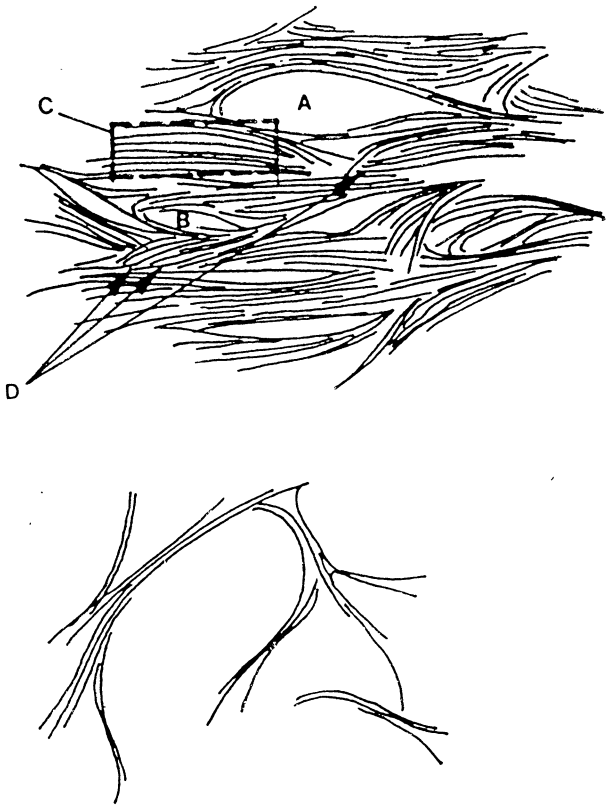

Figure 11. *Particle arrangements and presence of water of different nature in smectite. Upper: Stacks of lamellae separated by A) large more or less continuous voids with free water, B) small mostly isolated voids with some structured water, C) Interlamellar space with structured water, D) Edge-to face contacts between stacks. Lower: "Link-bond" between edge-to-face contacting smectite lamellae.*

3.2 Physical state and properties of porewater

The matter of physical state and properties of porewater has been examined and discussed since the birth of soil physics about a hundred years ago. As concerns smectite clays determination of density anomalies and various physico/chemical studies have led to the common opinion that interlamellar water has other properties than free water and that the external surfaces of smectite particles have a few hydrate layers adsorbed on them. Application of NMR technique and microstructural modeling of MX-80 has made it possible to determine and distinguish between relaxation properties of "internal" and "external" porewater [10]. These studies demonstrate that the interlamellar hydrates are in approximately the same ordered and highly viscous form independently of the total water content and that the mobility of interlamellar water molecules is significantly lower when Ca or Sr ions are in exchange positions than when the clay is in Na state. Heating from room temperature to about 80°C causes an increase in the relaxation time T_2 by 40-50 %, which means that the change in viscosity of the interlamellar water is much smaller than of the rest of the porewater. It is estimated from this fact that the number of interlamellar hydrates in buffer clay in Ca form remains unaffected if it is heated from room temperature to about 80°C under confined conditions, while there may be some moderate reduction of this number in Na buffer clay.

The general idea is that interlamellar water can be regarded as quasi-crystalline, viscous hydrates that have a "disjoining" function, in the sense that they connect the lamellae in the stacks and provide strength to them, and at the same time tend to separate the lamellae to form a maximum number of hydrate layers of 3 in Na clay and 2 in Ca clay, thereby contributing to the swelling pressure. When the average number of interlamellar hydrates is less than that the swelling pressure is very low and only provided by osmotic effects. The basal surfaces of the stacks have a hydrate coating consisting of one to three layers of less regularly organized water molecules when the crystallographic axes of neighboring stacks do not coincide. This water component and the rest of the water in the space between the stacks form the "external" water which has the same physical properties as free water.

3.3 Evaluation of interparticle bonds

Following Feltham et al [11,12] and applying general thermodynamics, the activation energy of the dominant rate process in creep of any material can be written as:

$$u^* = u_o - v\tau = m\mathrm{k}T \qquad (2)$$

where:

u^*	Thermally accessible energy barrier height
u_o	The intrinsic height of the barrier opposing shear, i.e. the strength of the major type of bonds
v	Activation volume (volume of flow unit)
τ	The applied shear stress
m	28**
T	Temperature
k	Boltzmann's constant

The creep equation is:

$$de/dt = \mathrm{A}\, e^{-(u_o - v\tau)/\kappa T} \qquad (3)$$

and for approximately constant v one obtains for two stress/strain sets:

$$v\tau = \mathrm{k}T[(\ln\varepsilon_2/\varepsilon_1)/\ln\tau_2/\tau_1] \qquad (4)$$

Figure 12 shows typical creep curves for MX-80 bentonite and they indicate that about 5E5 s after onset of creep the strain rate is approximately proportional to the applied stress, which means that the expression within brackets in Eq.4 equals unity. For earlier creep stages this value is higher and it also depends on the bulk density of the clay, which is explained by the larger number of interparticle bonds for higher densities. The bracketed expression has a value of about 2.3 for a time after onset of creep of 5E4 s using MX-80 clay with a density 1900 kg/m^3, while it is 1.3 for a density of 2000 kg/m^3.

Using Eq.(2) one finds u_o to be approximately 0.6 eV for long-term creep of MX-80 while it is on the order of 0.75 eV for clay with a content of illite particles of about 70 %. 0.6 eV is the average energy of hydrogen bonds (0.3-0.9 eV) while 0.75 eV represents the upper range of this spectrum. The higher value for illite may partly be due to other, stronger interparticle bonds like primary valence bonds, while the lower value for the smectite clay suggests that the majority of the interparticle bonding is provided by strongly adsorbed water. This is in agreement with the general belief that the large majority of the interparticle contacts are formed by mineral-adsorbed water as outlined above.

A similar approach was made by Leo Keinonen in 1973 [13], who investigated remolded illitic clay and found that the work needed for compression is related to the water sorption capacity, hence indicating that water films separate particle contacts in remolded clay and suggesting that hydrogen bonds are dominant ligaments also in illitic clay with aligned stacks of illite lamellae, i.e. with smectite-like microstructure. Applying thermodynamics, Keinonen determined

* This figure emanates from basic thermodynamic considerations and is discussed later in the paper

the free (Gibb's) energy of the porewater by measuring the negative pore pressure by use of tensiometers, centrifuges and vapor pressure gauges and predicted compression curves that turned out to agree very well with experimental ones.

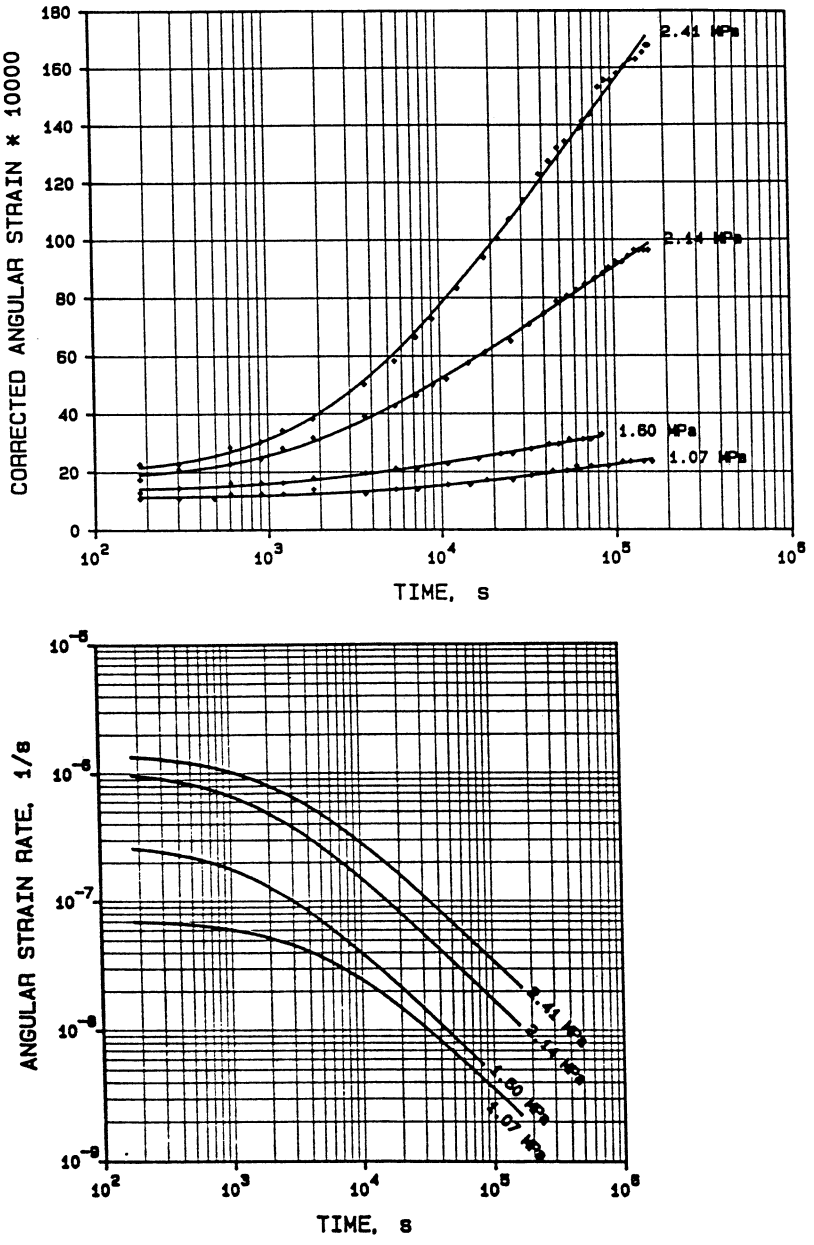

Figure 12. *Creep curves of MX-80. Upper: Creep strain versus time. Lower: Creep strain rate versus time.*

3.4 Interparticle bond spectrum

Figure 13 illustrates schematic particle arrangements in MX-80 clay as interpreted from electron microscopy. They imply that the interparticle distance and types of contact vary, which means that the interparticle bond strength varies according a spectrum with the lowest energy barriers being on the order of 0.1 eV and the highest ones representing the upper limit of the hydrogen bond, i.e. 0.9 eV [14]. Also the concept of microstructural variation manifested by the parameter data in Table 2 suggests a spectrum of the interparticle bond strength.

A spectrum of the interparticle strength exists also in apparently homogeneous clay because the particle distance varies and thereby the strength of the individual bonds and the dilatancy at shearing (Figure 13). The effect is not very important for dense clays since their microstructure is relatively homogeneous.

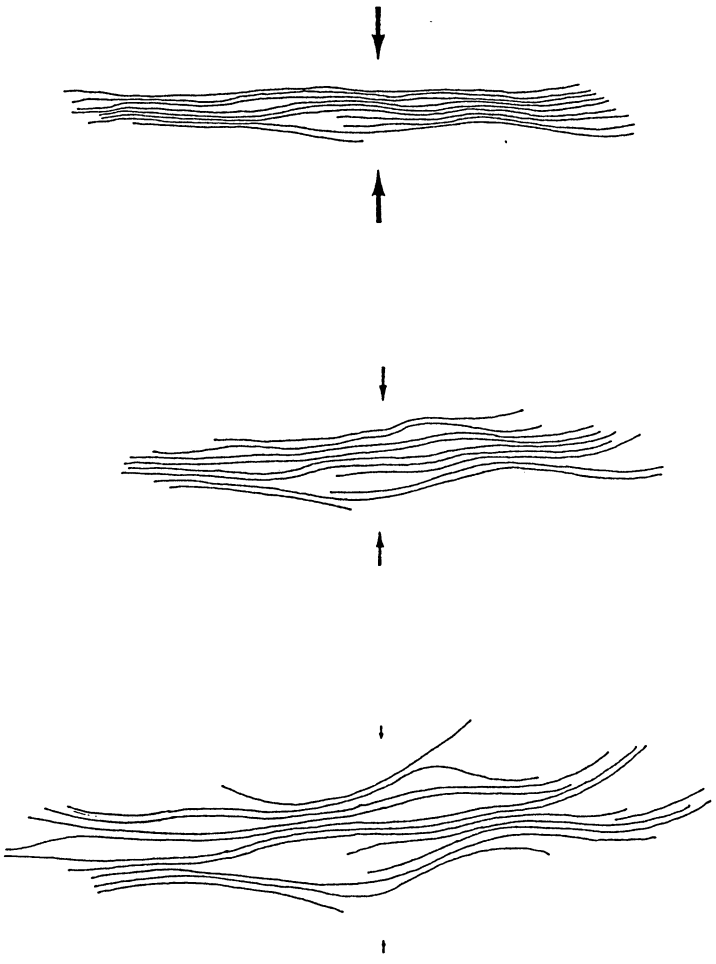

Figure 13. *Schematic picture of variations in microstructure of smectite clay at different effective pressures yielding a change from the state of complete interlamellar hydration (lowest) to a highly compressed state with locally no hydrates and 2-3 hydrates, respectively (upper).*

4 COMMON CREEP MODELS

4.1 Introduction

Creep means time-dependent strain of which there are three types in soils:

1. Compression of microstructural voids. This process, which is termed primary consolidation in soil mechanics, is particularly important for clays since their low hydraulic conductivity delays dissipation of the porewater overpressure caused by loading.

2. Compression of microstructural voids controlled by creep strain of the particle network. The strain rate is sufficiently low to make the associated expulsion of water take place with only insignificant porewater overpressure. This process is termed secondary consolidation in soil mechanics.

3. Shear strain under constant volume conditions. This process involves microstructural shear distortion and can be termed "constant volume creep".

Primary consolidation has the nature indicated in Figure 14 and it can be predicted by calculating the change in density that is generated by loading. For the particular case considered in the present report, i.e. the load exerted by the canister, it can be conservatively estimated by calculating the axial compression of the buffer clay located below the base of the canister, assuming that the total load is carried by the 0.5 m high clay column below the base. Taking the weight of the canister as 20 tons it will generate a pressure of about 0.22 MPa, hence increasing the existing effective pressure, which is equal to the swelling pressure, by this amount. The swelling pressure is taken here as 7 MPa for the bulk density 2050 kg/m^3, meaning that the resulting pressure 7.22 MPa may increase the density to about 2075 kg/m^3 at maximum. This change corresponds to a loss of water of the considered column of about 70 liters, yielding an axial compression of 30 mm. In practice, canister wall friction and stress distribution in the clay from the loaded area will yield a much smaller settlement; it will probably be less than 10 mm and is hence of no concern.

Secondary consolidation is included in the primary consolidation for expansive clays like the MX-80 and is therefore neglected.

The "constant volume creep" is the only time-dependent strain that needs to be considered in the present context. Its practical importance can be imagined by considering the buffer clay as a highly viscous substance, which deforms slowly under the shear stresses induced by the canister load but which can undergo very large strain in a long period of time if the viscosity is constant. The problem in

predicting long-term creep is that the detailed strain mechanisms have not been considered by most investigators and that only empirical creep data are available. In this paper common empirical models will be commented on and a creep model proposed that is believed to form a sufficiently strong basis for predicting creep over very long periods of time.

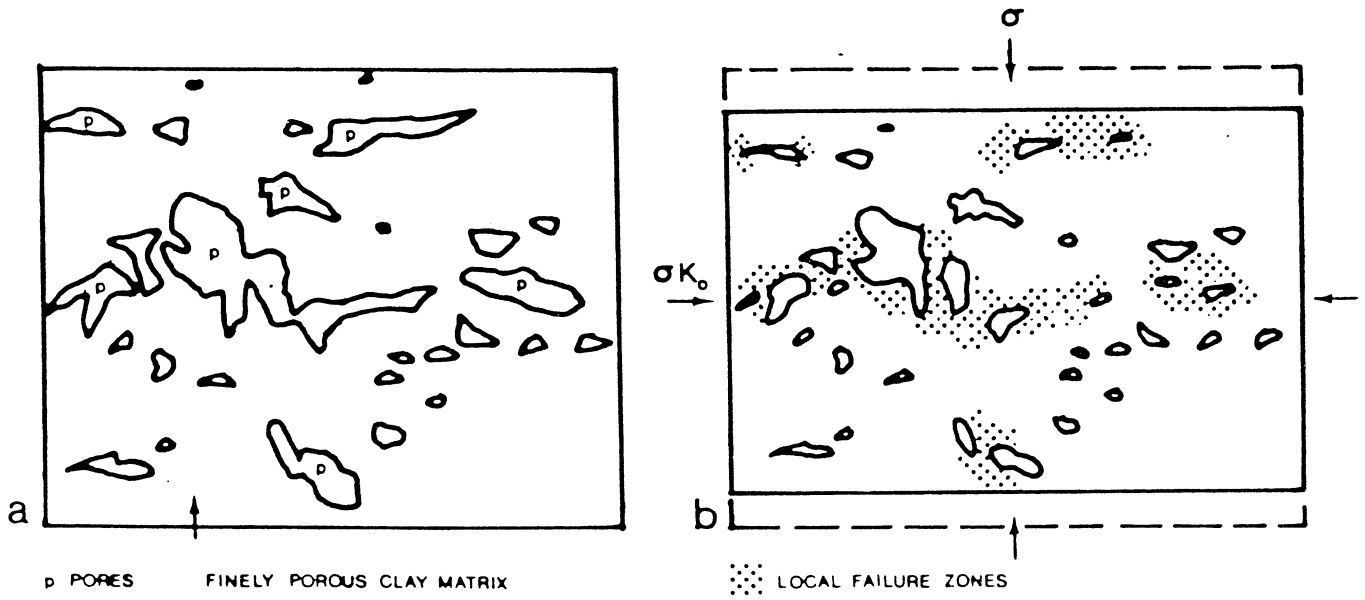

Figure 14. *Microstructural changes in the primary stage of consolidation [14]. Left (a): Undisturbed (initial) conditions. Right (b): Larger pores compressed in connection with local breakdown of the clay particle network.*

4.2 Mathematical form of current creep models

4.2.1 General

Empirically, the creep rate of clays can be expressed as in Eq.5 [1,15,16,17,18]:

$$d\gamma/dt = A\ T^a\ D^b\ (t)^n \qquad (5)$$

where

γ = Strain
D = Deviator (shear) stress
T = Absolute temperature
a, b, c, n = Exponents

t = Time after onset of creep

The very general form represented by Eq.5 makes recorded data fit well for a limited period of recording but the validity over longer periods of time for constant parameter values is doubtful. Neither the mathematical form nor the parameters reveal anything about the true nature of the creep process.

4.2.2 The stress parameter *D*

The stress conditions control the strain rate, firstly because the microstructural elements undergoing creep will be exposed to higher stresses when the overall stress state is increased, and secondly because microstructural changes may alter the internal geometry and cause local breakage by which less bonds will remain operative or by which the bonds may become weaker.

The importance of stress is well known and can be illustrated as in Figure 15, which shows the creep rate as a function of time after onset of creep of a clay for different shear stresses. The log-log diagram demonstrates that the curves are straight lines with an inclination that decreases with increased stress, and that the strain rate for a sufficiently high stress becomes constant and then increases, yielding failure. It is commonly assumed that creep may accelerate in the fashion indicated by curves *a* and *b* in Figure 15 if the shear stress exceeds about 2/3 of the conventionally determined value. Similarly, a shear stress lower than about 1/3 of this strength may drop quicker than indicated by the log time curves.

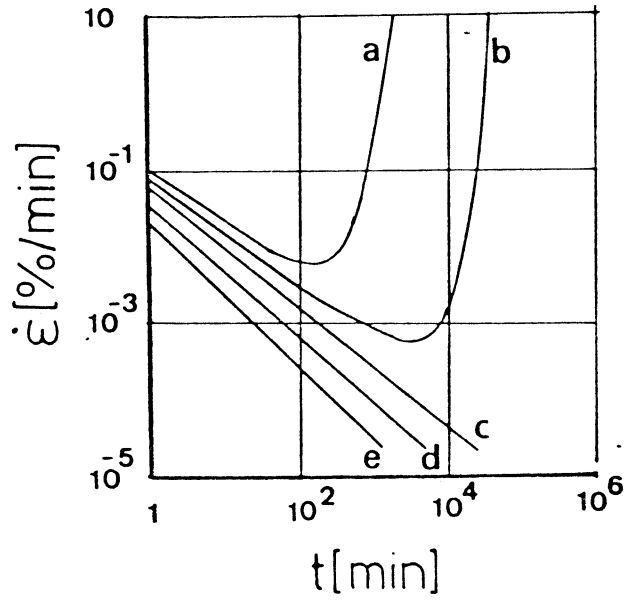

Figure 15. *Typical set of curves showing slope and shape changes when the shear stress is increased in separate tests on the same type of clay. The stress is increased in the order e<d<c<b<a [14].*

4.2.3 The time parameter *n*

For montmorillonite-rich clay with Na as dominant adsorbed cation represented by MX-80 n has been reported to range from -0.80 to -1.0 (mean value -0.91), putting the time function as $(t/t_r)^n$ where t_r is a reference time 16].

For the French candidate clay Fo-Ca7, which largely consists of expanding clay minerals, n ranges between -0.73 and -1.03 (mean value -0.88), [17].

For certain soils the exponent n is consistently lower than -1. Ice at around the freezing point obeys the so called Andrade creep (n=-2/3) and for frozen clay n is on the same order of magnitude, which is explained by the fact that the creep strain is controlled by the ice lenses that are typically formed by freezing [3].

A better fitting form of Eq.5 is Eq.6 where t_o is a structure-related parameter:

$$d\gamma/dt = A\ T^a\ D^b\ (t + t_o)^n \qquad (6)$$

In one of the most lasting, very carefully conducted creep experiments on stiff Na-smectitic (London) clay, Bishop recorded the creep data plotted in the diagram in Figure 16 [19]. It is found that the creep is proportional to the logarithm of $(t + t_o)$, as illustrated by Figure 16. The diagram shows two creep curves for different shear stresses, 40-47 % of the conventionally determined shear strength representing the left curve with t_o = 0.45 days, and 70-82 % of this strength for the right curve with t_o = 0.01 days.

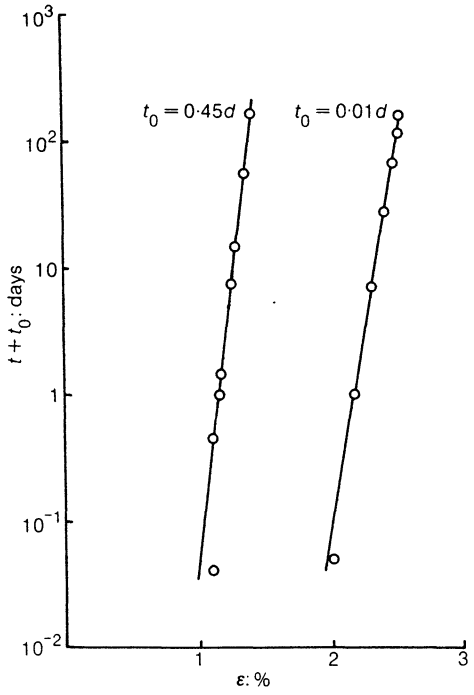

Figure 16. *Creep of stiff London clay under drained conditions [19].*

Figure 17 shows the meaning of the parameter t_o: one can interpret low t_o values as representing comprehensive microstructural response and quick adaptation to the general creep performance represented by $t_o = 0$, while high values indicate slow engagement of the microstructural network before the creep becomes "normal". Negative values are believed to represent very quick initial drop of the creep rate due to cementation [1,18]. These interpretations apply to the London clay experiments.

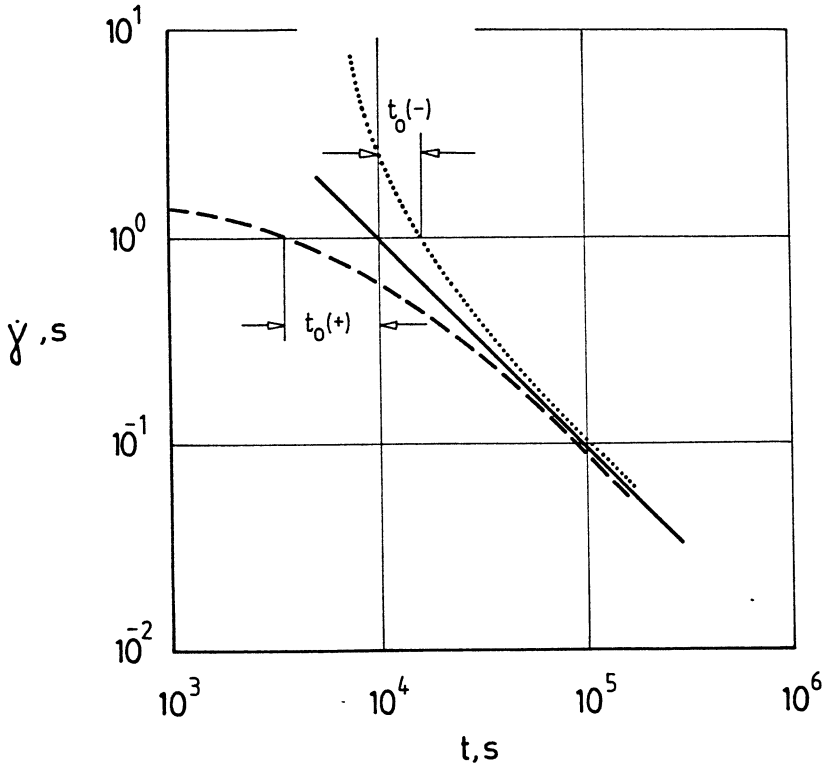

Figure 17. *Meaning of the t_o parameter [18].*

4.2.4 Criteria for a creep model for predicting long-term canister settlement

A creep model that is sufficiently reliable to be used for predicting canister settlement over very long periods of time should be derived on the basis of thermodynamics and have the form of a rate process model related to the microstructural behaviour. This is in fact the only possible way to develop a reliable creep theory, while empirical creep models have a validity that is confined to the length of the respective testing periods, i.e. a few years at maximum.

The present paper describes a model that is believed to fulfil the criteria.

5 CREEP MODEL PROPOSED FOR PREDICTING CANISTER SETTLEMENT

5.1 Introduction

The basic assumption made here is that a deviatoric stress, initially applied to a clay element, is held constant during the entire period over which the creep is being studied. The element is assumed to have been consolidated under isotropic stress conditions, which roughly corresponds to the conditions for the water saturated buffer clay in the deposition holes. The porewater pressure attendant to the incremental shear stress produced by the canister load is believed to be stress invariant and to dissipate in the course of the very slow strain process.

The characteristic features of the response of the microstructure to the shear stress are 1) overall deformation of the entire network of particles accompanied by 2) translations and rotations of dense aggregates and larger particles, and by 3) deformation of bridging aggregates and clay gels. The processes are illustrated in Figure 18 for the case with sufficiently large strain to yield ultimate failure.

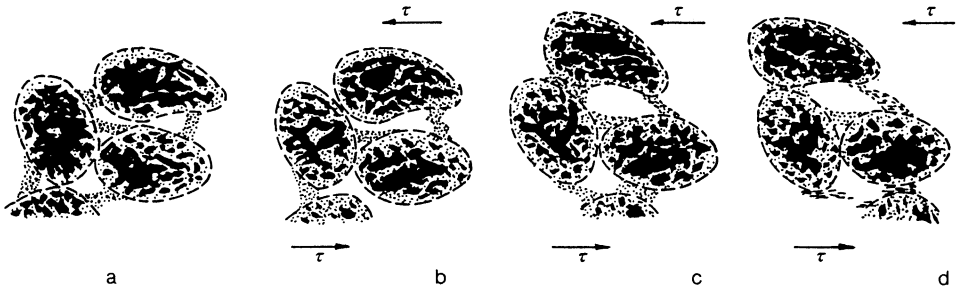

Figure 18. *Consecutive stages in the evolution of the creep structure of aggregated clay: a) Before loading, b) Instantaneous shear and formation of slip units in conjunction with movement of stiff aggregates and stacks of lamellae, c) Formation of slip domains accompanied by local healing and breakdown, d)Large strain wit creep failure [18].*

The destruction of water lattices and other bonds impair the resistance to slip and this will facilitate a rapid initial deformation at the onset of the creep. Two principal, partly compensatory, mechanisms will, however, combine to reduce the creep rate progressively. Firstly, local displacements cause stronger microstructural units to make contact and promotes formation of new bridging aggregates, which both help to strengthen the structure. Secondly, the

displacements lead to breakdown or weakening of originally bridging aggregates by altering their initial heterogeneous structure with more or less random orientation to become an aligned matrix of stacks of lamellae. The overall effect of the destructive and recovery processes is believed to depend on the average strain rate and hence on the stress level. The presently proposed creep model considers cases with a range of stress levels as well as the influence of chemical processes including cation exchange and cementation.

5.2 The stochastic model

5.2.1 Basic features

The aspects of creep as a rate process implying the existence of a spectrum of energy barriers are fundamental features of the model, which has been proposed by Feltham and Pusch and which is believed to be suitable for calculating shear-induced creep of clay under constant volume conditions [11,12].

As in other materials thermally activated slip is the most likely rate-determining process causing creep. In view of the heterogeneity of the material from the point of view of local stress and chemical structure, one has to consider that at a given point j where slip is held up at an energy barrier u_j that is determined by the intrinsic nature of the obstacle, u_{jo}, the local deviatoric stress τ_j acting on it at the time t determines whether continued strain will take place or not. The stress- and time-dependence of u_j can therefore be represented by Eq.7 and 8:

$$u_j = u_j(u_{jo}, \sigma_j) \tag{7}$$

$$\tau_j = \tau_j(t) \tag{8}$$

For the general case with different types and height of intrinsic barriers and taking ν_D as an atomic vibrational frequency of the order of 10^{12} per second, the jump frequency over a consecutive series of barriers of height u as given by classical rate theory would be the expression in Eq.9:

$$\nu(u) = \nu_D \exp(-u/kT) \tag{9}$$

If $\nu(u)$ is taken to be on the order of one second one gets $\nu(u) = 10^{12} \exp(-u/kT)$ from which one gets Eq.10:

$$u = m\mathrm{k}T \tag{10}$$

with m being about 28 for the temperature range in a repository.

The selection $v(u)$ to be one second is not arbitrary since for much higher jump rates the process would be completed to quickly to be observable, while with too infrequent jumps no creep would be observed even for very long periods of time. Allowing for a certain v-range Eq.10 implies that only a limited u-spectrum, like the 0.1 – 0.9 eV range for the H-bond, will be of significance. As concerns the number $\Delta(u,t)$ of potential slip elements per unit volume of material that are held up at time t at barriers of height u, the spectrum is considered as subdivided into equal intervals of width δu (Figure 19).

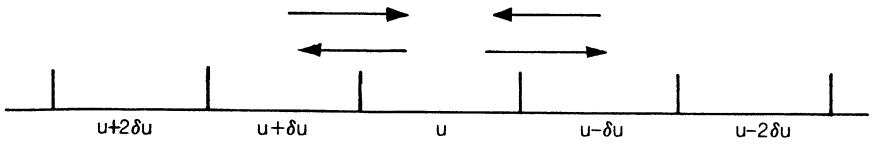

Figure 19. *Section of energy-barrier range with transitions in steps to and from a given u-level.*

For the general case of "normal" creep, slip activated at a certain point gives a contribution to the overall shear by the associated extension of the slip patch and the next barrier to be encountered will be either higher or lower by an average amount δu. Taking the probabilities of jumps to higher and lower barriers to be the same one obtains a diffusion-type differential equation for $n(u,t)$. Following Feltham et al [20] the solution of this equation implies that the spectrum $n(u,t)$ is proportional to $p\, e^{-p}$ where p has the form of Eq.11:

$$p = \exp(u/kT)/v_D(t + t_o) \qquad (11)$$

where t_o is a constant of integration.

Taking each activated jump to make the same mean contribution to the shear strain the theoretical deduction yields the commonly observed logarithmic type of creep, i.e. with creep strain being proportional to log $(t + t_o)$. A general mathematical form of the model is expressed by Eq.12:

$$d\gamma/dt = \beta\, T\tau/(t + t_o) \text{ with } \tau = \text{ constant} \qquad (12)$$

where β depends on the structure and thereby on the density.

It is concluded that the theoretical model expresses the creep strain in the same fashion as derived from many experiments, i.e. Eq.6, when the shear stress is of intermediate magnitude, i.e. between about 1/3 and 2/3 of the conventionally determined shear strength. Since the principal form of the creep equation in Eq.6 can hence be validated using thermodynamically based rate process theories it is reasonable to apply it to many geotechnical problems including the present issue of long-term canister settlement in dense smectite clay.

5.2.2 General performance of the model

One can illustrate the function of the creep model by applying a simple computer code (DENEB [21]) as demonstrated in [14]. The code is based on the assumption that the probability that a slip unit will have a sufficiently high kinetic energy Δu to overcome a barrier encountered is equal to $e^{-\Delta u/kT}$. If the frequency of jumps of the slip unit is ν the number of encounters in time Δt is $\nu\Delta t$, while the probability p that it will be held up by the barrier after this time is given by Eq.13:

$$p = (1- e^{-\Delta u/kT})^{\nu\Delta t} \qquad (13)$$

If a large number of independent slip units were located in independent potential wells, the fraction f that has overcome the barrier u is expressed by Eq.14:

$$f = 1- p = 1 - (1- e^{-\Delta u/kT})^{\nu\Delta t} \qquad (14)$$

The code implies that there are N energy barrier heights uniformly distributed between the lowest (u_1) and the highest (u_2) ones, and also that the slip units are initially uniformly distributed among the barriers. A further important assumption is that slip units that have overcome their current barrier are assumed to be held up at the next lower or higher barrier.

Applying the model to the case with all particle ligaments being hydrogen bonds with u_1=0.1 eV and u_2=0.9 eV and taking for the sake of simplicity the number of energy barrier heights to be 10 and the number of slip units to be 1000, one finds the successive redistribution of slip units held up at different energy barriers to be as shown in Figure 20. It illustrates the essence of the creep model, i.e. that slip units move up and down adjacent barriers but that the net effect is that they ultimately move up to and become held at the upper end of the barrier spectrum provided that a critical stress state has not been reached.

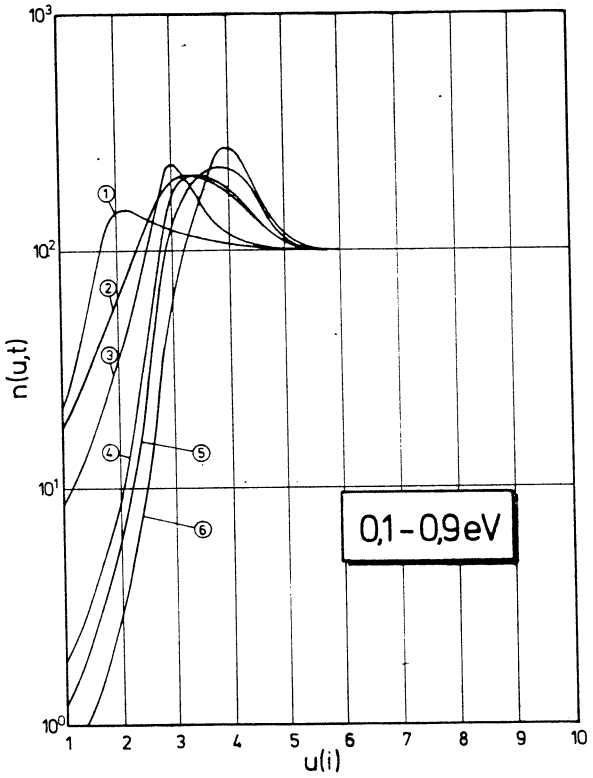

Figure 20. *Total number of slip units held up at different barriers after onset of creep. 1) 10^3 s, 2) $5x10^3$ s, 3) 10^4 s, 4) $5x10^4$ s, 5) 10^5 s, 6)) $2x10^5$ s [14].*

5.2.3 Influence of stress

A basic assumption applicable to homogeneous viscous media is that the displacement of an average slip unit is proportional to the average bulk shear stress. However, for microstructurally heterogeneous clays the conditions are much more complex since the local stresses not only move the respective slip units but also make them grow in two or three directions, which would imply an exponential stress dependence although not to the same degree for all stress levels. Thus, for intermediate shear stresses the total number of slip units may be relatively constant, the strain rate being controlled by the local shear forces yielding the distribution of strain that is implied by the stochastic model.

Even for higher stresses the amount of slip units may not be increased very much but the higher strain rate causes growth of the units, i.e. more destruction

and crossing of higher energy barriers. The total strain may therefore be the determinant of whether a critical state will be reached causing increased strain rate and ultimate failure.

When the shear stress is increased progressively from initially zero to beyond the "intermediate" level, the number and size of slip units can be assumed to grow, thus yielding an exponential stress dependence. The rather insignificant creep for very low stresses has two main reasons. One is that the displacement of the slip units is very small at low stresses and the other that low stresses activate fewer slip units. While for intermediate bulk shear stresses the number of slip units is determined by the outflux from any u-level of the energy spectrum into the adjacent higher energy interval and by simultaneous influx from the adjacent lower one, bulk shear stresses lower than about 1/3 of the conventionally determined shear strength will rather yield "uphill" than "downhill" jumps [12,22], which yields a differential equation for $n(t)$ that can be expressed as by Eq.15.

$$\delta n/\delta t = - (v\delta u)\, \delta[n \exp(-u/kT)]/\delta u \qquad (15)$$

with the previously defined symbols. This means that the creep strain rate is proportional to $(1 - t/t_a)$ with $t<t_a$ as boundary condition. The creep shear (angular) strain is then of the form in Eq.16:

$$\gamma = \alpha t - \beta t^2 \text{ with the condition } t < \alpha/2\beta \qquad (16)$$

There are many examples of such rapid reduction of the creep rate in metals and alloys and it has been reported that also clays [23] may behave in this way at low shear stresses. However, all the creep tests made on MX-80 clay, including those made at low bulk shear stresses, suggest that creep takes place according to the general model (Eq.6) rather than to the low-stress model characterized by Eq.16. The general creep model will therefore be used for predicting canister settlement since it represents more conservative conditions.

5.2.4 Influence of temperature

Considering the change in proton mobility expressed in terms of the relaxation time T_2 [10] one would expect the creep rate at 90°C to be about 50 % higher than at room temperature, while the creep model in Eq.6 implies that it should be only about 24 % higher assuming a linear relationship between temperature (Kelvin) and creep rate. The swelling pressure, which is believed to be a measure of the average strength of the clay and hence influencing the creep rate, should drop with increasing temperature and earlier tests have also indicated that the swelling pressure at 90°C is about 50 % of that determined at room temperature for clay saturated with distilled water and 70 to more than 100 % for

clay saturated with 0.3 M $CaCl_2$ solution (Table 3). It is expected on these grounds that the average creep rate may be significantly raised when the temperature is increased but that the ion exchange from Na to Ca that is foreseen will moderate this effect.

Table 3. *Influence of temperature on the swelling pressure (p_s) of water saturated MX-80 clay with no porewater overpressure[24] but with different porewater electrolytes*[1)].

Density at saturation kg/m^3	p_s, MPa. Room temp. Distilled water	p_s, MPa. Room temp. 0.3 M $CaCl_2$	p_s, MPa 90°C. Distilled water	p_s, MPa 90°C 0.3 M $CaCl_2$
1900	4-6	1-2	2-3	0.3-0.6
2000	7-12	5.0	4-7	3-7
2100	30.0	30.0	10-12	20-40

1) The data are higher than most recently determined values since different techniques were used but the relative change in pressure for the different temperatures is believed to be relevant.

5.2.5 Influence of porewater chemistry

The negligible difference between the microstructural parameter values of MX-80 clay saturated with distilled water to a bulk density of 2000 to 2100 kg/m^3 and those of clay saturated with salt water (3.5 % $CaCl_2$ solution), and the insignificant difference between the physical properties of these clay forms, as well as the rather small difference in relaxation properties of their interlamellar water, suggest that the creep behavior of such dense clay should be rather independent of the porewater chemistry.

This is supported by comparing creep tests of MX-80 clay saturated with distilled water and calcic Forsmark groundwater (1.1 % salt content), respectively [18]. These tests gave the creep parameter values summarized in Table 4, indicating that the two clay forms have similar creep properties for the stress interval 0.5 – 0.6 MPa except that the Ca-clay has higher t_o:s. This indicates that it takes longer time for activating the slip units in the stronger Ca-saturated clay. The table also shows that the parameter values change significantly when the shear stress exceeds about 2/3 of the shear strength.

The parameters A and B refer to Eq.17, which is based on Eq.6 taking the creep to be proportional to temperature and stress [18]. These two factors are expressed by the B-parameter while A is a material (integration) constant. For the present purpose the strain refers to the canister settlement Δ.

$$\Delta = B \ln (t + t_o) + A \qquad (17)$$

Table 4. *Creep parameters of MX-80 clay with a density at saturation of 2100 kg/m^3 modeled according Eq.17 [18]. The bulk shear strength is 1000 kPa.*

Clay form	**Ratio of shear stress and bulk strength, MPa**	***A****	***B****	t_o, **s**
Distilled water	0.45	-13.8	3.7	1075
	0.56	-22.7	6.7	612
(Shear strength	0.67	-48.7	11.2	453
2.4 MPa)	0.78	-111.6	22.4	468
3.5 % $CaCl_2$	0.37	-20.8	3.8	5168
solution	0.55	-20.7	4.7	1615
	0.73	-114.1	17.8	1641
(Shear strength	0.83	-262.5	36.2	2492
2.9 MPa)	0.92	-	915	10500

* The values must be multiplied by 10^{-4}

For a density of about 2100 kg/m^3 at water saturation, which approximately represents the presently considered buffer clay, the data in Table 4 give the relationship between "mobilized" shear strength, i.e. the ratio of average bulk shear stress and the bulk strength, and the parameters A and B that are approximated by Eqs.18 and 19, which are valid for the interval Λ<0,6.

$$A = (100\ \Lambda - 5)\ \text{E}{-4} \qquad (18)$$

where Λ is the the ratio of average bulk shear stress and the bulk strength.

$$B = \Lambda\ (\text{E-3}) \qquad (19)$$

t_o is characterized by a polynome-type function with two maxima, one for low and one for high Λ:s but for "intermediate" stresses it can be taken as 500 s for Na bentonite saturated with electrolyte-poor water, and 1500 s for Ca bentonite in rough but conservative estimates of canister settlement. For lower Λ–values than 0.3 t_o is significantly higher.

5.2.6 Influence of mineral changes

The expected mineralogical changes in the heating period of the water saturated buffer clay are primarily a slow conversion of the smectite component montmorillonite to non-expanding clay, and cementation by dissolution of the smectite and silicious accessory minerals, especially feldspars, in the hot part of the buffer clay and precipitation of hydrous silica/aluminum in the colder part.

The firstmentioned process may have the form of solid solution conversion via mixed-layer minerals or by dissolution yielding free silica and aluminum which produce neoformed illite at a rate that is controlled by the influx of external potassium [25]. Changes in creep behavior are expected to be due to changes in the number and strength of the interparticle bonds, for which a possibly altered density is believed to be a major factor since it affects the continuity of the particle network. Literature data give typical illite densities of 2650 kg/m^3 [26] while that of montmorillonite is usually taken as about 2700 kg/m^3.

The difference in mineral density at complete conversion to illite is hence insignificant and not believed to be of importance, while the redistribution of the clay density on the microstructural level may have an impact on the bulk strength and creep behavior of the buffer clay. Thus, assuming solid state conversion to illite, the stacks of smectite with an average number of interlamellar hydrates of 1-2, which corresponds to the bulk density 2050 kg/m^3, will contract so that their thickness will drop by about 15 %. The average width of adjacent voids will thereby increase, which will result in more continuous water flow paths and a loss in effective stress. The latter is illustrated by the experimentally determined swelling pressure 0.5 MPa of illitic clay (illite 40 %, quartz and feldspars 30 %, chlorite 15 %, calcite 10 %) with a density of 2100 kg/m^3 [18]. MX-80 with the same density has a swelling pressure of at least 5 MPa.

The undrained shear strength of this illite-dominated clay is on the order of 100 kPa, i.e. only about 5 % of that of MX-80 clay [18], which hence suggests that the creep rate of illite-converted buffer will increase very significantly. However, the rate of mineral conversion is concluded to be very low and not lead to a lower smectite content than about 50 % in the first 100 000 years using the working model proposed for predicting alteration of smectite to non-expanding minerals [10]. Changes in creep rates due to smectite-to-illite conversion will therefore have no practical impact on the engineered barriers.

Cementation is being considered as a possible mineral alteration process associated with illitization since it has been identified in natural heat-exposed bentonite beds. It means that time-induced strain will not be initiated until a threshold stress has been reached and that the strain is less than in non-cemented clay once the critical stress has been exceeded [18]. A recent study related to the Kinnekulle bentonite has indicated that cementation by silica precipitation makes smectite clay brittle and less expansive and that this natural clay underwent alteration very rapidly, i.e. in a thousand years. This is believed to have been caused by the high temperature (100-140°C for 700 years) and by comprehensive groundwater flow for supplying the bentonite with the required amount of potassium [27]. Since such flow will not be possible according to the performance criteria of the KBS-3 concept, illitization and cementation are believed to be very minor and of negligible practical importance. If cementation takes place at all it will rather slow down creep strain than increase it.

5.2.7 General comments

The creep model described here is based, in principle, on thermodynamics and stochastic theory. The latter is needed considering the very large number of particles and the wide bond energy spectrum that are due to the nature of the clay material and the physico/chemical processes taking place on the molecular level. The basic Eq.6 defining the creep rate as derived from the conceptual model and its equivalent in closed form, Eq.17, for the strain imply linear dependence of temperature and stress on the creep rate, which has not yet been proven but seems to be reasonable or even conservative. The matter is further discussed in conjunction with the description of experiments simulating canister settlement.

6 PREDICTION OF CANISTER SETTLEMENT

6.1 Background

The matter has been investigated in two earlier studies based on simple assumptions concerning the parameters of the creep model. The present paper summarizes the earlier results and the outcome of laboratory and field tests, and contains a prediction of the settlement made for the present project by Dr Robert Adey, BEASY, using the boundary element method and applying relevant parameter values.

6.2 Laboratory-scale experiments

6.2.1 Program

Bench-scale experiments (1:20) were conducted in 1985, simulating the water saturation phase of precompacted buffer with a density at saturation of 2100 kg/m^3 and recording the creep settlement of a small centrally placed copper cylinder [28]. The weight of this 50 mm diameter miniature canister was simulated by applying a dead load of 80 kg for measuring the settlement rate after about 3 months of water absorption of the clay from the filter-equipped cylindrical container that represented rock. This period of time was needed for reaching practically 100 % water saturation.The settlement was recorded with an accuracy of +/- 0.1 μm. The maximum induced shear stress was about 15 % of the shear strength.

A series of tests was performed, starting with a 75 days long period of loading the clay at 22°C , followed by heating of the entire test set-up with the load left on to 50°C for 22 days. The temperature was then lowered to 22°C again for 255 days after which heating to about 70°C took place for 130 days, followed by a third room temperature period of 70 days. The complex thermo-mechanical behavior of the system involving transient heat-induced expansion and cooling-induced contraction of the confining cylinder and the clay with porewater made it difficult to evaluate the entire creep evolution but the periods of "steady-state" creep after reaching isothermal conditions and dissipation of porewater overpressure gave useful results. The shear strength and bulk density of the water saturated clay was 1 MPa and 2100 kg/m^3, respectively.

6.2.2 Step 1 (T=21.5-22.0°C)

The sudden application of the load caused visco-elastic strain and initial displacements due to the establishment of mechanical contact between the components and also some consolidation, but one finds from Figure 21 that already after a few hours regular log time settlement took place yielding a

settlement of about 6 μm after 75 days. Taking the settlement to be 2.5 μm per decade it is concluded that continued creep strain according to this creep law will be on the order of 18 μm in 30 000 years.

6.2.3 Step 2 (50°C temperature)

After the initial complex thermo-mechanical processes, which appeared to last for about one week and which involved expulsion of porewater and quick settlement of the canister by about 70 μm, the settlement proceeded with the same rate as at room temperature (Figure 21).

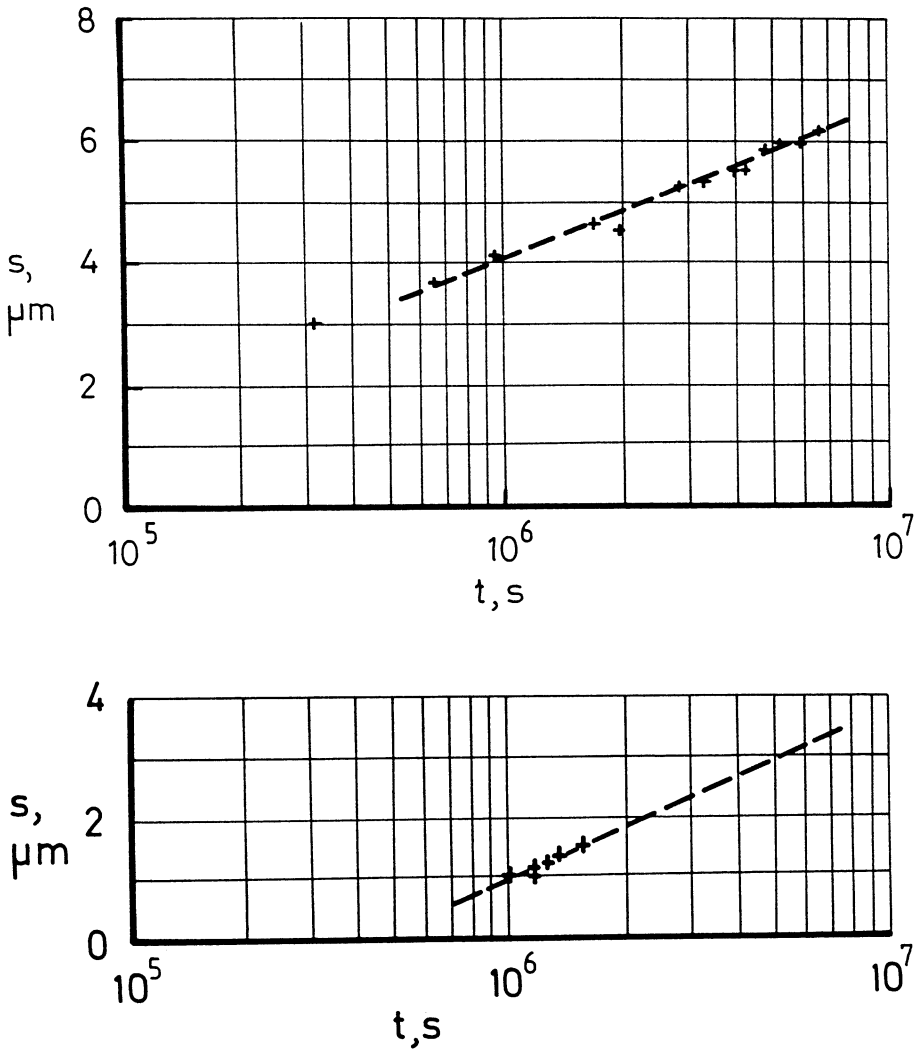

Figure 21. *Recorded settlement of the model canister. Upper: Room temperature conditions. Lower: Settlement after heating to about 50°C.*

6.2.4 Step 3 (T=21.5-22.0°C)

After the initial complex thermo-mechanical processes, which appeared to last for about one week and involved uptake of water and quick upheaval of the canister by about 30 μm, the settlement proceeded with the same rate as at room temperature.

6.2.5 Step 4 (T=69.6-69.9°C)

After the initial complex thermo-mechanical processes, which appeared to last for about one week and involved expulsion of water and quick settlement by about 250 μm of the canister, settlement continued according to a $\log(t+t_o)$ relationship (Figure 22). At the end of the about 3 months long period the settlement took place at a rate of about 3 μm in 100 days, which would mean about 18 μm in about 30 000 years, or about the same as that for room temperature.

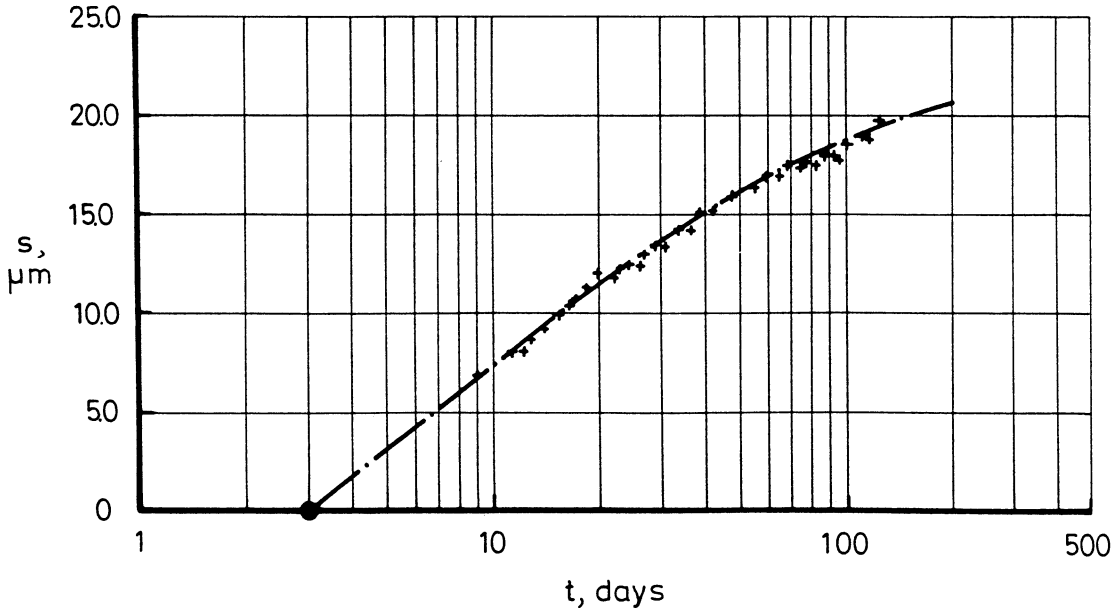

Figure 22. *Recorded settlement of the model canister after heating to about 70°C.*

6.2.6 Comments on the bench-scale tests

The bench-scale tests showed that heating produces significant thermo-mechanical displacements and porewater overpressure if the buffer is fully water saturated at the start of the heating. After thermal equilibrium and dissipation of the porewater overpressure, the settlement appeared to follow a creep law of the type $\log(t+t_o)$ with about the same creep parameters at room temperature and at 70°C. It can be expected that heating to 90° may increase the creep rate somewhat but it seems reasonable to assume that the linear relationship between temperature and creep rate postulated by Eq.6 represents a conservative case.

The settlement was predicted by numerical calculations using boundary element technique and applying Eq.20, which is a special case of Eq.6 (t_o=0). The calculations gave a settlement curve for the testing period that agreed very well with the recorded one [29].

$$ds/dt = \beta\, T\, D\, \ln t \qquad (20)$$

where:

s = settlement
β = strain parameter evaluated from undrained triaxial tests (3E-10 to 2E-8 K^{-1} kPa^{-1} for the density interval 2100 to 1900 kg/m^3).

$D = \sigma_1 - \sigma_2$ (σ representing principal stresses)
$\sigma_2 = \sigma_3$

Calculations using an early version of the BEASY boundary element code [28] gave very good agreement with the recorded settlement as illustrated by Table 5, which supports the belief that the general creep model expressed in terms of Eq.6 can be used for describing and predicting creep of the buffer if consolidation is omitted and the shear stresses on the same order of magnitude as in the buffer clay in the deposition holes.

Table 5. *Predicted and actual settlement of model canister under isothermal conditions with T=20°C. (β=3E-10 K^{-1} kPa^{-1}).*

Time after onset of creep, s	**Predicted settlement, μm**	**Recorded settlement, μm**
3E5 (0.01 years)	3	3.0
6E5 (0.02 years)	4	3.7
3E6 (0.1 years)	5	5.2
6E6 (0.2 years)	6	6.0

6.3 Field experiment

A 1:5 scale test was performed in the Stripa mine from mid 1986 to the end of 1988 [30]. Due to the canister geometry a load of 8.5 t would have been required to balance the difference in swelling forces on its upper and lower ends when the water saturation of the 0.1 m clay annulus and 0.2 m thick clay layer below the canister had become practically complete. However, the applied load was only about 90 % of the theoretically derived figure because of lack of accuracy in laboratory-derived swelling pressure data at that time and the field test hence showed that the canister underwent heave rather than settlement. A further reason for heave was that the upper part of the 0.4 m diameter borehole, in which the test was made, was backfilled with a bentonite/sand mixture with low density. It was hence compacted by the upward expanding buffer clay which moved the canister upwards.

The major finding from the experiment was that heating of the canister to about 93°C caused significant expansion of the porewater of the clay, which contributed to the canister heave. Also, it was concluded that settlement caused by consolidation would be several times larger than the settlement caused by creep under constant volume conditions.

6.4 Prediction of canister settlement using improved model

6.4.1 General

A further developed version of the BEASY code was used by Computational Mechanics Ltd, Southampton, UK, for predicting the settlement of a 20 t canister embedded in MX-80 buffer clay with a bulk density of 2050 kg/m^3 at saturation. The calculations, which are fully described in an Appendix to this report, referred to the theoretical condition of instantaneous emplacement of the canister in fully water saturated clay, omitting consolidation. Cases with and without upward expansion of the buffer were considered.

6.4.2 Geometry

The diameter and height of the canister were taken to be 1.05 m and 4.8 m, respectively. The clay below the canister was taken to be 0.5 m at the beginning of the strain process and 1.5 m over the top of the canister. The thickness of the clay annulus surrounding the canister walls was taken to be 0.35 m. The clay/canister system was assumed to be contained in a 1.75 m diameter vertical hole with 7 m depth in rigid rock. Its upper end was assumed to be closed by a fixed boundary in Case I and open to upward creep movement in Case II.

6.4.3 Basic assumptions for the calculations

Two basically different conditions were investigated: Slip along all clay/rock and clay/canister boundaries, and no slip at any boundary. The firstmentioned may be relevant for the case of no canister corrosion or if easily yielding corrosion products are formed at the canister surface, while the second may correspond to the case of very stiff corrosion products being formed at the canister surfaces.

The clay was given a modulus of elasticity of 300 MPa, which is the value obtained by applying the common rule for stiff clays that the modulus is about 300 times the undrained shear strength. The constant volume conditions were fulfilled by applying the value 0.49 for Poisson's ratio. Room temperature conditions were assumed, meaning that the creep-enhancing 2000 year long heat pulse and the expected lower temperatures in forthcoming glaciation periods were disregarded.

The basic creep law was Eq.17 with A=-E-3 and B=2E-4, and with t_o=2500 s.

6.4.4 Results

The results, which are summarized in Table 6, mean that the largest settlement will produced assuming no slip at any boundary. However, the settlement is very small and negligible from a practical point of view, i.e. 0.762 mm. Taking the temperature to about 90°C and the actual canister weight (25 000 kg) into consideration the total settlement in E4 years may be about 1 mm and possibly a couple of millimeters in E6 years. Creep-induced settlement is hence very small in comparison with the consolidation and the various thermo-mechanical processes. The initial canister heave will mask these processes and leave the insignificant creep as major strain mechanism a few decades after emplacing the canisters in the deposition holes. Tectonics and glaciation loads will in fact have a stronger impact on the buffer and canister in a long term perspective.

Table 6. *Results of settlement calculations (See Appendix). Settlement in mm.*

Time, years	**Confined case (I), Slip**	**Confined case (I), No slip**	**Open case (II), No slip**
E0	0.358	0.049	0.051
E1	0.426	0.058	0.060
E2	0.493	0.068	0.070
E3	0.560	0.077	0.079
E4	0.627	0.086	0.089
E5	0.695	0.095	0.098
E6	0.762	0.105	0.108

One finds from the displacement graphs in the Appendix that the large majority of the shear strain takes place below and adjacent to the canister base and that only very little strain occurs higher up above the base than a few decimeters. This is reconfirmed by the data in Table 6 which show very little difference between the confined and open cases. The finding that almost no strain is transferred to the upper part of the canister-embedding buffer hence means that practically all buffer deformations above the canister will be related to the expansion of the buffer that produces compression of the overlying backfill.

7 DISCUSSION AND CONCLUSIONS

7.1 The viscosity analogy

The strain- or time-dependent changes of the stress distribution on a molecular level that are basic to Eqs.6 and 17 can be described qualitatively and quantitatively by use of rheological models with successively increased numbers of activated slip units, like the Blizard-Cauer ladder structure (Figure 23). It is based on the basic Kelvin model [18] but needs to be generalized for practical application. The physical performance of the ladder model can be represented by Eyring's version with a successively increased resistance to flow being caused by a non-linear viscous element (Figure 24) and introducing the simplification that the viscosity of the dash-pot increases linearly with time in Eyring's model and removing one of its elastic elements, one arrives at the model in Figure 25, which will be used here.

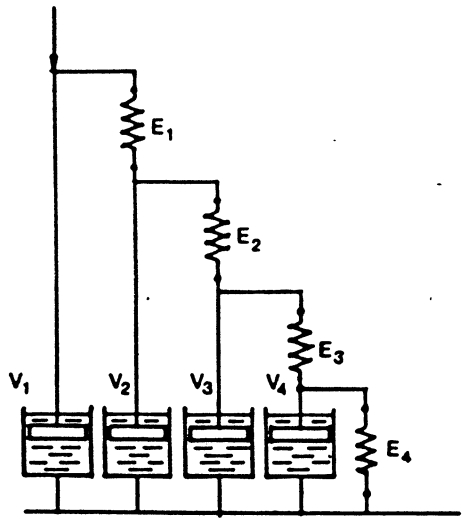

Figure 23. *Blizard-Cauer finite ladder structure with elastic elements E and viscous elements V. The number of elements with lumped parameters can be increased to infinity.*

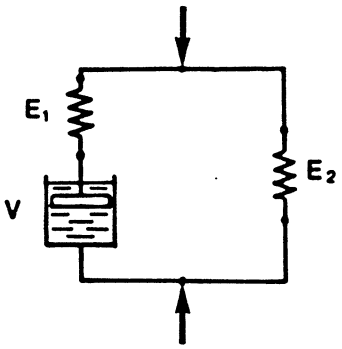

Figure 24. *Eyring's model with a non-linear viscous (dash-pot) element.*

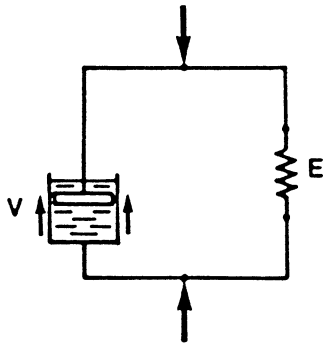

Figure 25. *Modified Eyring model with parallel elastic and non-linear viscous elements.*

The constitutive equations of the model are the following:

$$\sigma_E + \sigma_\eta = \sigma_o \tag{21}$$

$$\varepsilon_E = \varepsilon_\eta \tag{22}$$

where:

σ_o = instantly applied stress σ_E in the elastic element and σ_η in the viscous element. ε_E is the elastic strain and ε_η the strain of the viscous element.

The model implies the following differential equation:

$\eta(t)\varepsilon + E\varepsilon = \sigma_o$ with the condition $\varepsilon = 0$ for t = time = 0. (23)

The postulated proportionality between viscosity and time can be set as:

$\eta(t) = \alpha t + \eta_o$ (24)

where η_o is the initial viscosity, which yields the expression:

$(\alpha t + \eta_o)\varepsilon + E\varepsilon = \sigma_o$ (25)

This equation has the solution:

$\log\varepsilon = -(1 + E/\alpha) \log(t + \eta_o/\alpha) + \log[(\sigma_o \eta_o)^{E/\alpha} (\alpha)^{-(1+E/\alpha)}]$ (26)

which, for $\alpha >> E$ and $\alpha > 100E$, yields:

$\log\varepsilon = - \log(t + \eta_o/\alpha) + \log(\sigma_o/\alpha)$ (27)

This latter equation is equivalent to Eq.17 and one finds the identities:

$t_o = \eta_o/\alpha$ and (28)

$B = [(\sigma_o \eta_o)^{E/\alpha} (\alpha)^{-(1+E/\alpha)}]$ (29)

The dependence of α on B and the way in which t_o is related to η_o/α are illustrated by the diagram in Figure 26, taking σ_o to be 1 MPa as a reference value. One finds the creep curves to be of the same type as in typical tests illustrated by the graphs in Figure 12 with the same implication for t_o as the analytical model. However, η_o is obviously higher than 10^{12} Pas and a more reasonable value is 10^{14} Pas considering the much lower shear stress (about 0.15 MPa compared to 1 MPa in Figure 12). This initial viscosity and an E-value of about 300 MPa, as well as a t_o-value of 2500 s like in the numerical calculation, are reasonable parameters to be taken as input to viscoelastic settlement calculations.

A very simple estimate of the settlement using the model in Figure 25 would yield a total ultimate settlement of around 1 mm as controlled by the elastic

element, the movement being retarded in the same rapid fashion as the stochastic model, i.e. about 50 % of the settlement being developed in 10 years, 75 % in 1000 years and about 95 % in 10 000 years. A special code based on the material model in Eq.27 has to be developed for adequate calculation.

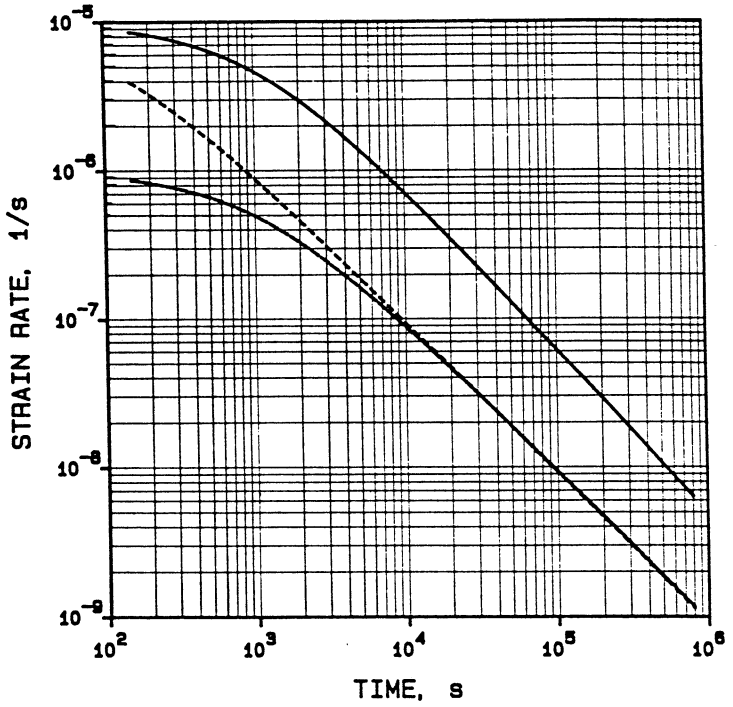

Figure 26. *Examples of theoretical creep curves derived for the modified Eyring model. The three curves are characterized by the following data sets:*

Upper: E = 10 MPa, η_o = E11 Pas, α = E8, t_o = E3 s
Central: E = 10 MPa, η_o = E11 Pas, α = E9, t_o = E2 s
Lower: E = 10 MPa, η_o = E12 Pas, α = E9, t_o = E3 s

7.2 Major conclusions from the study

The study has shown the following:

- Commonly used soil creep models are empirical and not valid beyond the period of time for which the underlying experiments have been conducted, i.e. a few years.

- The huge number of particles and the wide range of the particle bond spectrum of the buffer clay require use of stochastical mechanics in establishing relevant creep models, and the physical nature of the constituents, especially the adsorbed water, must be incorporated by

considering thermodynamics. These features are basic to the creep model proposed for predicting creep settlement.

- The influence of the stress level on the creep strain of MX-80 clay is not known with certainty but for the stress interval valid for the buffer the assumption of strain being proportional to stress is concluded to be conservative.

- The influence of temperature on the creep strain of MX-80 clay is not well known. Theoretical considerations based on heat-induced changes in the proton relaxation time suggest a very moderate impact for temperatures up to 90°C and this is supported by model experiments. It is believed that the assumption of strain being proportional to temperature is conservative.

- Mineral alteration will be of minor importance for the creep in the first tens of thousands of years. Cementation by dissolution/precipitation may take place to some extent, possibly causing some reduction in creep rate.

- The shear-induced creep settlement under constant volume conditions calculated by using the proposed creep model is on the order of 1 mm in ten thousand years and up to a couple of millimeters in one million years.

- The estimated consolidation settlement, which takes place early and which is masked by various initial strain components, i.e. canister upheaval due to temperature-induced expansion of the clay and upward swelling, is much larger than the creep settlement under constant volume conditions. It is believed to be on the order of 10 mm or slightly less.

- **The general conclusion that is drawn from the study is that creep settlement of the canisters is very small and of no significance to the integrity of the buffer itself or of the canisters.**

8 REFERENCES

1. Pusch R et al, 1995. Handbook of Buffers and Backfills, Part I. SKB Arbetsrapport AR 95-45, SKB Stockholm.

2. Pusch R, Muurinen A, Lehikoinen J, Bors J, Eriksen T, 1999. Microstructural and chemical parameters of bentonite as determinants of waste isolation efficiency. Final Report of EC-contract No.:F14W-CT95-0012. The EC Commission, Brussels.

3. Pusch, R, Karnland, O, Hökmark, H, 1990. GMM- A general microstructural model for qualitative and quantitative studies of smectite clays. SKB Technical Report TR 90-43, SKB Stockholm.

4. Pusch R, 1962. Clay particles. Swed. Build. Res. Council, Stockholm.

5. Swartzen-Allen S L, Matijevic E, 1974. Surface and colloid chemistry of clays. Chemical Reviews, Vol.74, No.3 (pp.385-391).

6. Lagaly G, 1989. Characterization of flow of kaolin and bentonite dispersions. Applied Clay Science, Vol.4 (pp.105-123).

7. Pusch R, 1999. Experience from preparation and investigation of clay for microstructural analysis. Engineering Geology Vol. 54, Nos 1-2 (pp. 187-195).

8. Yong R N, Warkentin B, 1975. Soil Properties and Behaviour. Elsevier Publ. Co, Amsterdam.

9. Pusch R, 1978. Engineering aspects of clay-weathered Blekinge gneiss. Geologiska Föreningens i Stockholm Förhandlingar, Vol.101 (pp. 27-31).

10. Pusch R, 1993. Evolution of models for conversion of smectite to non-expandable minerals. SKB Technical Report TR 93-33.

11. Feltham P, 1979. The inter-relationship: earth sciences-material sciences. Mechanisms of deformation and fracture. Pergamon Press, London (pp. 29-42)

12. Pusch R, Feltham P, 1980. A stochastic model of the creep of soils. Geotechnique, Vol.30, No.4 (pp. 497-506).

13. Keinonen L, 1973. An energetic model of consolidation in cohesive soils. Proc. 8th International Conference on Soil Mechanics and Foundation Engineering, Moscow 1973, Vol.1 (pp 203-207).

14. Pusch R, 1979. Creep of soils. Ruhr-Universität Bochum, Schriftenreihe des Instituts fuer Grundbau, Wasserwesen und Verkehrswesen, Serie Grundbau Heft 5.

15. Singh A, Mitchell J K, 1968. General stress-strain-time functions for soils. American Society of Civil Engineers, Proc. Vol.94, No SM1.

16. Börgesson L, Hökmark H, Karnland O, 1988. Rheological properties of sodium smectite clay. SKB Technical Report 88-30. SKB, Stockholm.

17. Börgesson L, Pusch R, 1987. Rheological properties of a calcium smectite. SKB Technical Report TR 87-31, SKB Stockholm.

18. Pusch R, Börgesson L, Erlström M, 1987. Alteration of isolating properties of dense smectite clay in repository environment as examplified by seven pre-Quaternary clays. SKB Technical Report TR 87-29, SKB Stockholm.

19. Bishop A W, 1966. The strength of soils as engineering materials. Geotechnique Vol.16, No.2 (pp.91-128).

20. Feltham P, 1973. A stochastic model of crystal plasticity. Applied Physics, Vol.6 (pp.2048-56).

21. Feltham P, Miles G, 1976. DENEB – A computer code for numerical integration of the equations governing the thermal activation of discrete, independent dislocation segments across energy barriers. Int. Report Dept. of Physics, Brunel University, England.

22. Pusch R, 1978. Creep mechanisms in clay. Proc. Interdisciplinary Conference on Mechanisms of Deformation and Fracture. International Series on the Strength and Fracturebof Materials and Structures, Ed. K. Easterling. Pergamon Press.

23. Pusch R, 1979. Creep mechanisms in clay. Proc. 3rd Int. Conf. On Numerical Methods in Geomechanics, Aachen 2-6 April, Editor W. Wittke, Vol.1 (p-491).

24. Pusch R, 1980. Swelling pressure of highly compacted bentonite. SKBF/KBS Technical Report 80-13. SKB, Stockholm.

25. Pusch R, Madsen F, 1995. Aspects on the illitization of the Kinnekulle bentonites. Clays and Clay Minerals, Vol.43, No.3 (pp. 261-270).

26. Grim R E, 1953. Clay Mineralogy. McGraw-Hill Publ. Co, London.

27. Pusch R, Takase H, Benbow S, 1998. Chemical processes causing cementation in heat-affected smectite – the Kinnekulle bentonite. SKB Technical Report TR-98-25, SKB, Stockholm.

28. Pusch R, 1986. Settlement of canisters with smectite clay envelopes in deposition holes. SKB Technical Report TR 86-23, SKB Stockholm.

29. Pusch R, Adey R, 1986. Settlement of clay-enveloped radioactive canisters. Applied Clay Science, Vol.1 (pp. 353-363).

30. Börgesson L, Pusch R, 1989. Interim report on the settlement test in Stripa. SKB Technical Report TR 89-29, SKB, Stockholm.

APPENDIX

BEM-CALCULATION OF CANISTER SETTLEMENT

By Robert Adey

Computational Mechanics International Ltd
Ashurst Lodge, Southampton, UK

BEM-CALCULATION OF CANISTER SETTLEMENT

Definition of problem.-

Calculate the instantaneous (elastic) and time-dependent settlement of a cylindrical canister weighing 20 tons that is embedded in water-saturated buffer clay with a density of 2050 kg/m^3 located in a vertical bored hole in granitic rock. Only shear strain is considered, i.e. the clay is assumed to be almost incompressible (Poison's ratio= 0.49). The settlement was calculated for the time period 0 to 10^6 years (t=10, 100, 1000, 10000, 100000, 1000000 years). The canister was assumed to be placed instantly in the clay and creep was assumed to start immediately afterwards.

Geometry.-

- The canister has a diameter of 1.05 meters and a height of 4.8 meters. The weight (in air) is 20 Tons and the density is 4811.94 kg/m^3.
- The canister is embedded in homogeneous clay with a density of 2050 kg/m^3. The clay below the canister base is initially 0.5 m thick and above its top it is initially 1.5 m thick. The thickness of the clay annulus surrounding the canister walls is 0.35 m.
- The clay-embedded canister is located in a hole with 1.75 m diameter in very stiff rock. The length of the vertical hole is assumed to be 7 m. In case 0, slip was assumed between the canister and the clay and between the clay and the bedrock. Its upper end was assumed to have a stiff lid in one calculation (Case I) and to be open in a second calculation (Case II).

Conditions.-

- Apart from case 0, No slip takes place between the clay and the canister and between the clay and the rock.
- The clay has a modulus of elasticity of 300 MPa. Poisson's ratio can be taken as 0.49 for the elastic and delayed strain.
- The canister and rock can be considered to be perfectly rigid.
- The clay obeys the creep law described below.

$$\gamma = B\ln(t + t_0) + A$$

Where:

γ= shear strain (dimensionless)= 0.1×10^6 Pa (experimental)

$A = -1 \cdot 10^{-3}$

$B = 2 \cdot 10^{-4}$

A and B have been evaluated from shear tests with the average shear stress being about 1/10 of the shear strength, which is about 1MPa. Time(t) was in second(s).

t_0= 2500 s

- The Average Deviator = $\frac{\int_v Ddv}{\text{Volume}} = \frac{\sum_1^{56} D_i v_i}{\text{Volume}}$

D= Deviator Stress = $\sigma_1 - \sigma_2$

σ_1 = The larger (i.e. more positive) of the principal stresses in the rz-plane.

σ_2 = The smaller (i.e. more negative) of the principal stresses in the rz-plane.

Volume= volume under the canister, between the canister and the bed of rock.

Resolution.-

In order to calculate $\int_v Ddv$ an array of 56 internal points were placed under the canister. At each of these points BEASY computed the complete stress tensor. It was required to write a program to take the output from the BEASY analysis, calculate the required principal stresses and deviator, and integrate the deviator over the volume.

CASE 0.

It was assumed to have slip between the canister and the clay and between the clay and the bedrock

It was taken just one zone with the following properties:

- Zone 1= Lines 1, 2, 3, 4, 5 ,6
- *Body forces.-*
  Acceleration 0.0000000E+00 -9.8100004E+00 0.0000000E+00 (m/s^2)
- *Zone properties.-*
  Youngs Modulus 3.0000000E+08 Pa.
  Poissons Ratio 4.9000001E-01
  Density 2.0500000E+03 (kg/m^3)
- *Boundary conditions.-*
  Normal displacement = 0 → lines 1, 2, 3, 5
  Traction = -226584.7 Pa → line 6

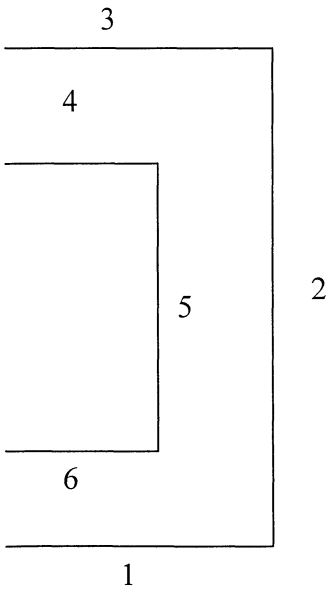

- Resolving $\int_v Ddv = \sum_1^{56} D_i v_i$, where $D = \sigma_1 - \sigma_2$ for each internal point.

Internal Point	$\sigma 1$(Pa)	$\sigma 2$(Pa)	D(Pa)	v(m^3)	D(Pa) x v(m^3)
1	-191760	-227230	35470	0.000966	34.2782
2	-175870	-229510	53640	0.000966	51.8377
3	-161700	-230800	69100	0.000966	66.7783
4	-150800	-230540	79740	0.000966	77.0607
5	-143530	-229350	85820	0.000966	82.9365
6	-139560	-228240	88680	0.000966	85.7004
7	-138410	-228160	89750	0.000966	86.7344
8	-191990	-227210	35220	0.002899	102.1098
9	-175460	-229250	53790	0.002899	155.9480
10	-160970	-230030	69060	0.002899	200.2188
11	-150030	-229160	79130	0.002899	229.4137
12	-142840	-227410	84570	0.002899	245.1854
13	-138970	-225920	86950	0.002899	252.0855
14	-137900	-225640	87740	0.002899	254.3759
15	-192340	-227170	34830	0.004832	168.2986
16	-174510	-228660	54150	0.004832	261.6528
17	-159410	-228340	68930	0.004832	333.0698
18	-148420	-226220	77800	0.004832	375.9297
19	-141450	-223410	81960	0.004832	396.0308
20	-137830	-221170	83340	0.004832	402.6989
21	-136900	-220520	83620	0.004832	404.0519
22	-192620	-227070	34450	0.006765	233.0474
23	-172670	-227550	54880	0.006765	371.2523
24	-156760	-225410	68650	0.006765	464.4036
25	-145880	-221400	75520	0.006765	510.8778
26	-139360	-217080	77720	0.006765	525.7603
27	-136180	-213860	77680	0.006765	525.4898
28	-135480	-212720	77240	0.006765	522.5132
29	-192350	-226860	34510	0.008698	300.1542
30	-169300	-225540	56240	0.008698	489.1531
31	-152630	-220680	68050	0.008698	591.8718
32	-142290	-214240	71950	0.008698	625.7924
33	-136620	-208200	71580	0.008698	622.5743
34	-134100	-203900	69800	0.008698	607.0926
35	-133760	-202240	68480	0.008698	595.6117
36	-190480	-226350	35870	0.01063	381.3125
37	-163120	-221750	58630	0.01063	623.2605
38	-146480	-213210	66730	0.01063	709.3667
39	-137610	-204300	66690	0.01063	708.9415

Internal Point	σ1(Pa)	σ2(Pa)	D(Pa)	v(m^3)	D(Pa) x v(m^3)
40	-133340	-196790	63450	0.01063	674.4990
41	-131760	-191560	59800	0.01063	635.6980
42	-131870	-189360	57490	0.01063	611.1418
43	-183680	-224730	41050	0.012563	515.7194
44	-151840	-213930	62090	0.012563	780.0492
45	-137980	-201800	63820	0.012563	801.7836
46	-132070	-191710	59640	0.012563	749.2694
47	-129800	-183660	53860	0.012563	676.6541
48	-129370	-177750	48380	0.012563	607.8077
49	-130010	-174830	44820	0.012563	563.0827
50	-156670	-215160	58490	0.014496	847.8712
51	-133270	-196470	63200	0.014496	916.1474
52	-127900	-185960	58060	0.014496	841.6379
53	-126380	-177960	51580	0.014496	747.7038
54	-126430	-171070	44640	0.014496	647.1016
55	-127230	-165000	37770	0.014496	547.5140
56	-128400	-160270	31870	0.014496	461.9876

$$\int_v D dv = \sum_1^{56} D_i v_i = 25300.54 \text{ Kg}\cdot\text{m}^2/\text{s}^2$$

- A= Area of the base of the cylinder = 0.866 m^2.
- t_0= 2500 s
- h= clay below the canister = 0.5 m.
- Volume= 0.433 m^3.

- Average Deviator = $\dfrac{\sum_1^{56} D_i v_i}{\text{Volume}} = \dfrac{25300.54}{0.866 \cdot 0.5} = 58430.8$ Pa

- Shear Stress= $\dfrac{\text{Average Deviator}}{2} = 29215.4$ Pa

- Scaling the experimental and our values for the equation $\gamma = B\ln(t + t_0) + A$.

$$\gamma = \frac{\text{Shear Stress}}{\text{Shear Stress (experimental)}} [B\ln(t + t0) + A]$$

- The settlement of the canister $\delta = h \times \gamma$

$$\delta = h \cdot \left[\frac{\text{Shear Stress}}{\text{Shear Stress (experimental)}} [B\ln(t + t_0) + A] \right]$$

$$\delta = 0.5 \cdot \left[\frac{29215.4}{1 \cdot 10^{5}} \left[2 \cdot 10^{-4} \ln(t + 2500) - 1 \cdot 10^{-3} \right] \right]$$

Calculating this equation for difference times, results in the following table:

t(years)	t(seconds)	Δ_{av}(m)	Δ_{av}(mm)
1	31536000	3.584E-04	0.358
10	315360000	4.256E-04	0.426
100	3.154E+09	4.929E-04	0.493
1000	3.154E+10	5.602E-04	0.560
10000	3.154E+11	6.275E-04	0.627
100000	3.154E+12	6.947E-04	0.695
1000000	3.154E+13	7.620E-04	0.762

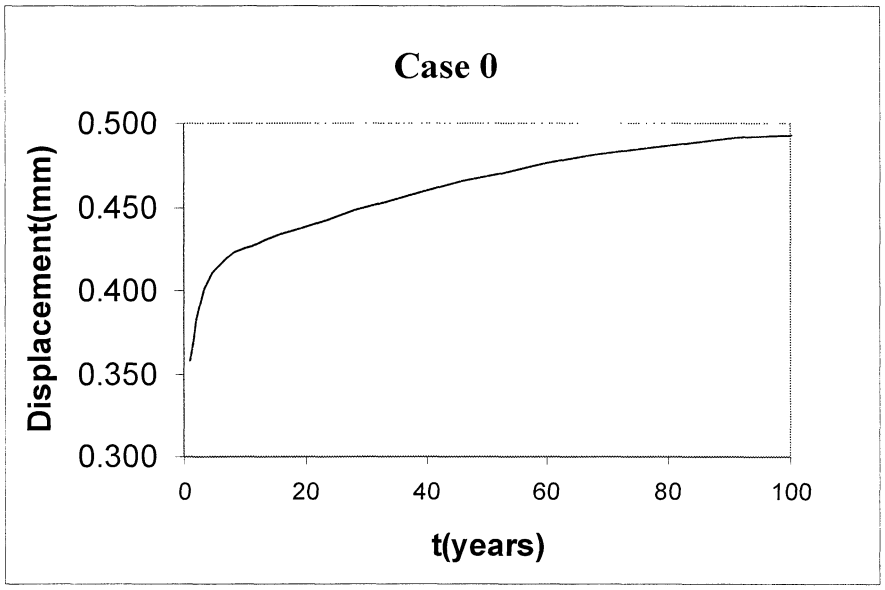

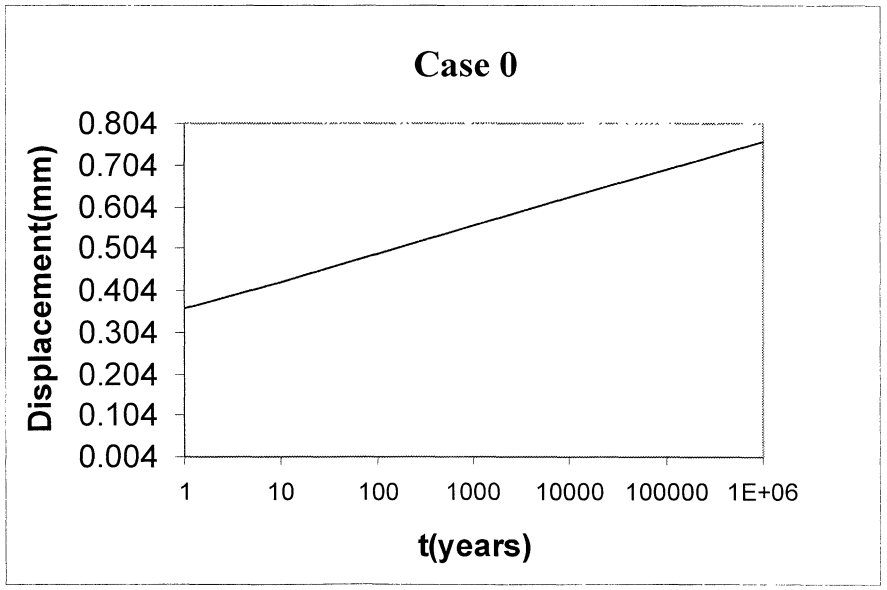

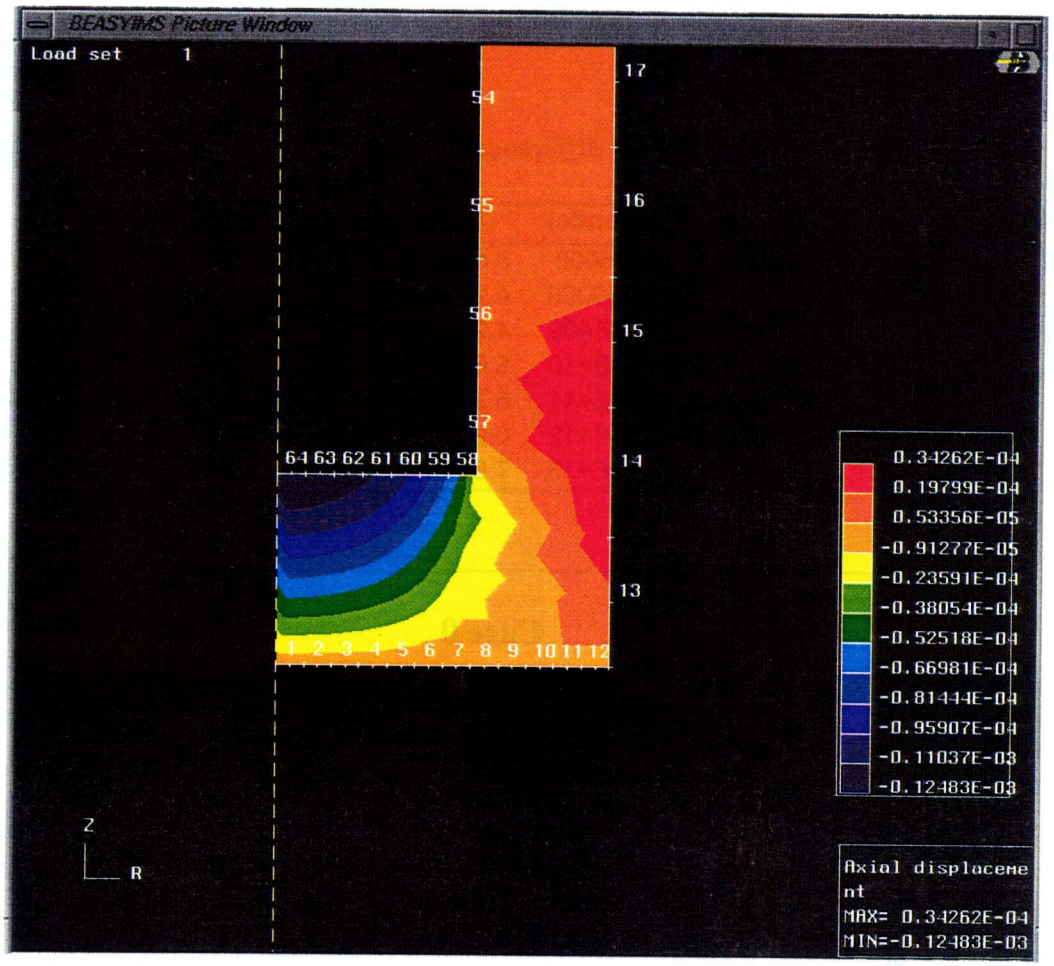
BEASYMS Picture Window
Load set 1
54
55
56
57
64 63 62 61 60 59 58
17
16
15
14
13
1 2 3 4 5 6 7 8 9 10 11 12
0.34262E-04
0.19799E-04
0.53356E-05
-0.91277E-05
-0.23591E-04
-0.38054E-04
-0.52518E-04
-0.66981E-04
-0.81444E-04
-0.95907E-04
-0.11037E-03
-0.12483E-03
Z
R
Axial displaceme
nt
MAX= 0.34262E-04
MIN=-0.12483E-03

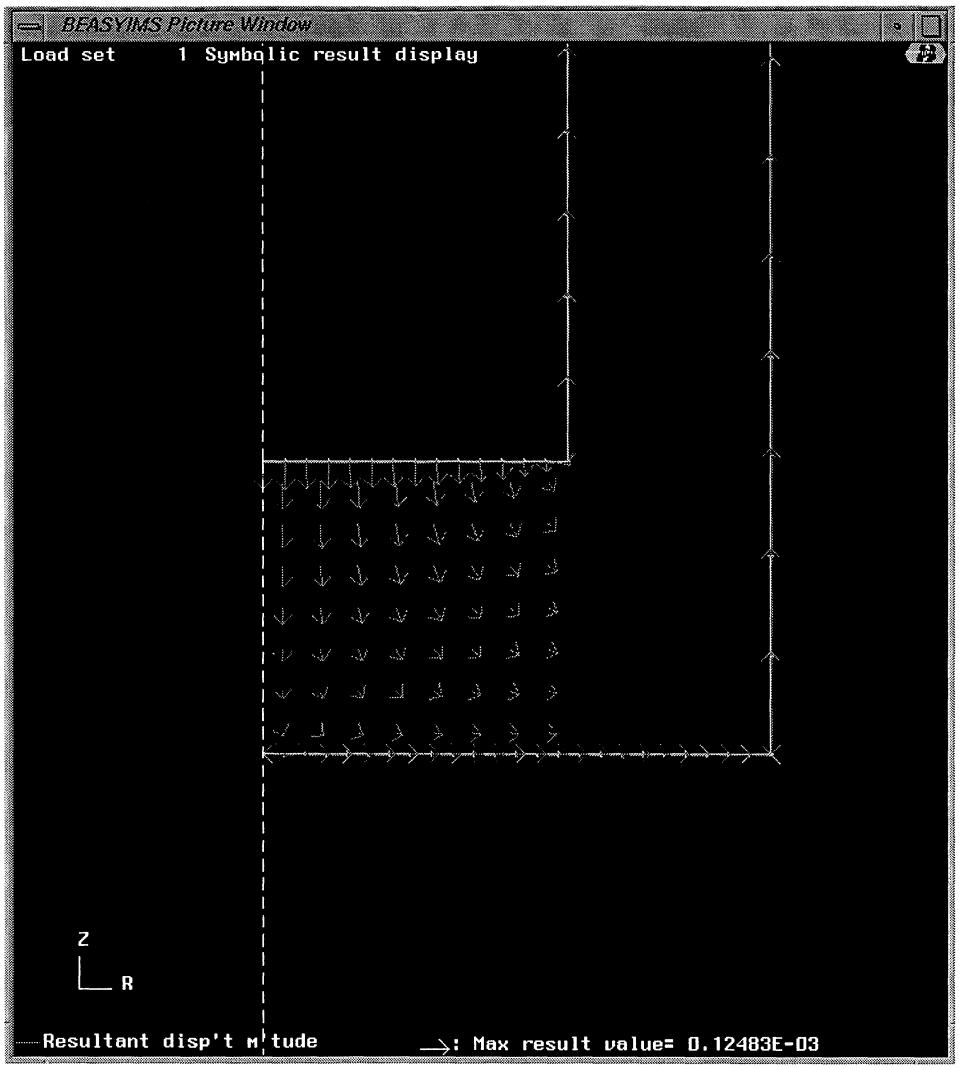
BEASYIMS Picture Window
Load set 1 Symbolic result display
Z
R
Resultant disp't magnitude
: Max result value= 0.12483E-03

CASE I.

No slip case. Its upper end was assumed to have a stiff lid.
It was taken two zones with the following properties:

- Zone 1= Lines 1, 2, 3, 4, 5, 6
- *Body forces.-*
  Acceleration 0.0000000E+00 -9.8100004E+00 0.0000000E+00 (m/s^2)
- *Zone properties.-*
  Youngs Modulus 3.0000000E+08 Pa.
  Poissons Ratio 4.9000001E-01
  Density 2.0500000E+03 (kg/m^3)
- *Boundary conditions.-*
  Normal displacement = 0 → lines 1, 2, 3.
  Z displacement=0 → line 4

- Zone 2= Lines 15, 5 ,6
- *Body forces.-*
  Acceleration 0.0000000E+00 -9.8100004E+00 0.0000000E+00 (m/s^2)
- *Zone properties.-*
  Youngs Modulus 3.0000000E+09 Pa.
  Poissons Ratio 3.0000001E-01
  Density 4.8119409E+03 (kg/m^3)

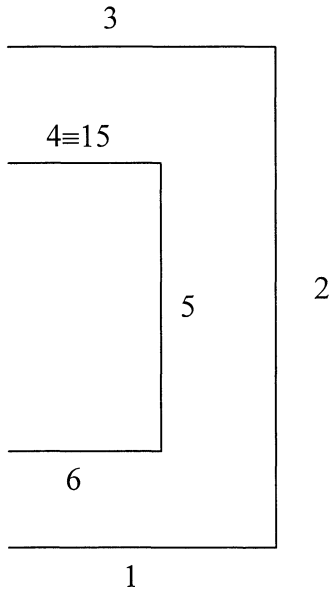

- Resolving $\int_v Ddv = \sum_1^{56} D_i v_i$, where $D = \sigma_1 - \sigma_2$ for each internal point.

Internal Point	σ1(Pa)	σ2(Pa)	D(Pa)	v(m^3)	D(Pa) x v(m^3)
1	-101370	-104390	3020	0.000966	2.9185
2	-100840	-106470	5630	0.000966	5.4408
3	-100560	-108380	7820	0.000966	7.5572
4	-100620	-110070	9450	0.000966	9.1325
5	-101040	-111600	10560	0.000966	10.2052
6	-101810	-113020	11210	0.000966	10.8333
7	-102900	-114440	11540	0.000966	11.1523
8	-101340	-104440	3100	0.002899	8.9875
9	-100790	-106470	5680	0.002899	16.4675
10	-100490	-108340	7850	0.002899	22.7587
11	-100540	-109990	9450	0.002899	27.3974
12	-100960	-111470	10510	0.002899	30.4706
13	-101740	-112860	11120	0.002899	32.2391
14	-102830	-114250	11420	0.002899	33.1089
15	-101300	-104560	3260	0.004832	15.7523
16	-100680	-106500	5820	0.004832	28.1222
17	-100340	-108270	7930	0.004832	38.3178
18	-100380	-109810	9430	0.004832	45.5658
19	-100820	-111190	10370	0.004832	50.1078
20	-101610	-112510	10900	0.004832	52.6688
21	-102720	-113860	11140	0.004832	53.8285
22	-101240	-104750	3510	0.006765	23.7445
23	-100510	-106550	6040	0.006765	40.8594
24	-100090	-108160	8070	0.006765	54.5919
25	-100120	-109520	9400	0.006765	63.5891
26	-100590	-110740	10150	0.006765	68.6627
27	-101420	-111950	10530	0.006765	71.2334
28	-102550	-113250	10700	0.006765	72.3834
29	-101180	-105050	3870	0.008698	33.6597
30	-100230	-106630	6400	0.008698	55.6646
31	-99718	-107960	8242	0.008698	71.6856
32	-99765	-109050	9285	0.008698	80.7572
33	-100290	-110080	9790	0.008698	85.1495
34	-101180	-111160	9980	0.008698	86.8021
35	-102330	-112400	10070	0.008698	87.5848
36	-101140	-105560	4420	0.01063	46.9864
37	-99777	-106740	6963	0.01063	74.0195
38	-99162	-107590	8428	0.01063	89.5930
39	-99284	-108330	9046	0.01063	96.1626

Internal Point	σ1(Pa)	σ2(Pa)	D(Pa)	v(m^3)	D(Pa) x v(m^3)
40	-99920	-109140	9220	0.01063	98.0123
41	-100890	-110120	9230	0.01063	98.1186
42	-102090	-111300	9210	0.01063	97.9060
43	-101070	-106570	5500	0.012563	69.0976
44	-98934	-106650	7716	0.012563	96.9377
45	-98348	-106800	8452	0.012563	106.1842
46	-98681	-107230	8549	0.012563	107.4028
47	-99496	-107910	8414	0.012563	105.7068
48	-100580	-108820	8240	0.012563	103.5208
49	-101840	-109990	8150	0.012563	102.3901
50	-100050	-108120	8070	0.014496	116.9827
51	-97262	-105360	8098	0.014496	117.3886
52	-97258	-105240	7982	0.014496	115.7071
53	-97997	-105700	7703	0.014496	111.6627
54	-99059	-106420	7361	0.014496	106.7051
55	-100280	-107350	7070	0.014496	102.4867
56	-101600	-108520	6920	0.014496	100.3123

$$\int_v Ddv = \sum_1^{56} D_i v_i = 3472.68 \text{ Kg}\cdot\text{m}^2/\text{s}^2$$

- A= Area of the base of the cylinder = 0.866 m^2.
- t_0= 2500 s
- h= clay below the canister = 0.5 m.
- Volume= 0.433 m^3.

- Average Deviator = $\dfrac{\sum_1^{56} D_i v_i}{\text{Volume}} = \dfrac{3472.68}{0.866 \cdot 0.5} = 8020.05$ Pa

- Shear Stress= $\dfrac{\text{Average Deviator}}{2} = 4010.02$ Pa

- Scaling the experimental and our values for the equation $\gamma = B\ln(t + t_0) + A$.

$$\gamma = \frac{\text{Shear Stress}}{\text{Shear Stress (experimental)}}\left[B\ln(t + t0) + A\right]$$

- The settlement of the canister δ= h x γ

$$\delta = h \cdot \left[\frac{\text{Shear Stress}}{\text{Shear Stress (experimental)}}\left[B\ln(t + t_0) + A\right]\right]$$

$$\delta = 0.5 \cdot \left[\frac{4010.02}{1 \cdot 10^5}\left[2 \cdot 10^{-4} \ln(t + 2500) - 1 \cdot 10^{-3}\right]\right]$$

Calculating this equation for difference times, results in the following table:

t(years)	t(seconds)	Δ_{av}(m)	Δ_{av}(mm)
1	31536000	4.919E-05	0.049
10	315360000	5.842E-05	0.058
100	3.154E+09	6.766E-05	0.068
1000	3.154E+10	7.689E-05	0.077
10000	3.154E+11	8.612E-05	0.086
100000	3.154E+12	9.536E-05	0.095
1000000	3.154E+13	1.046E-04	0.105

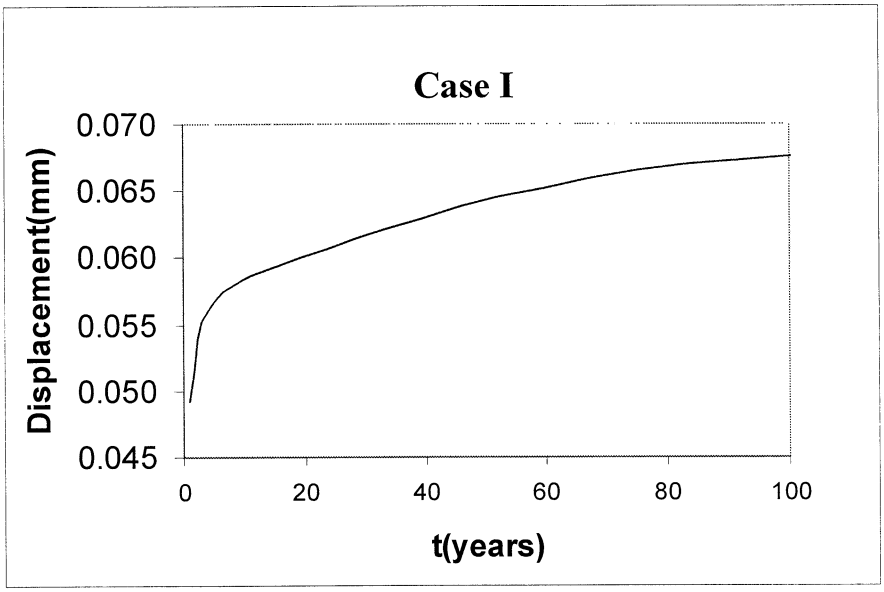

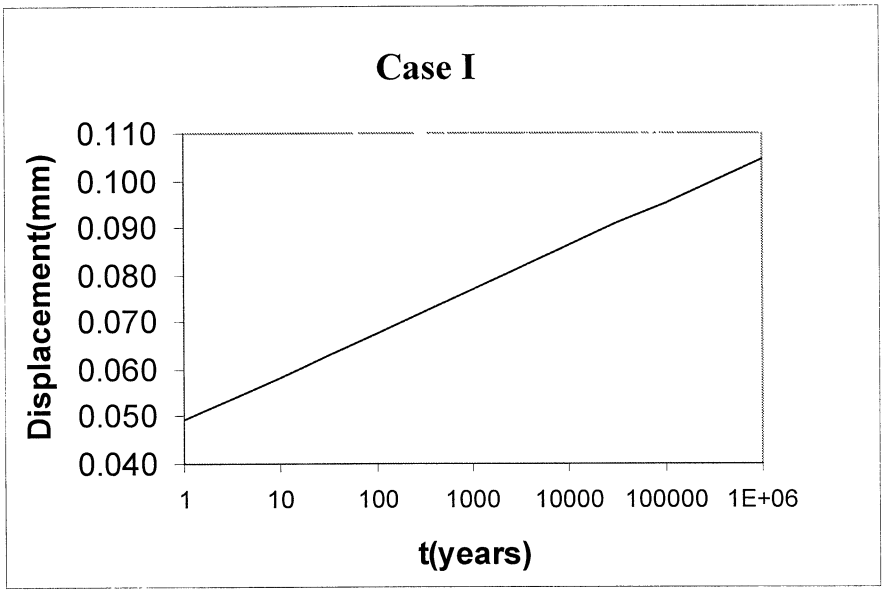

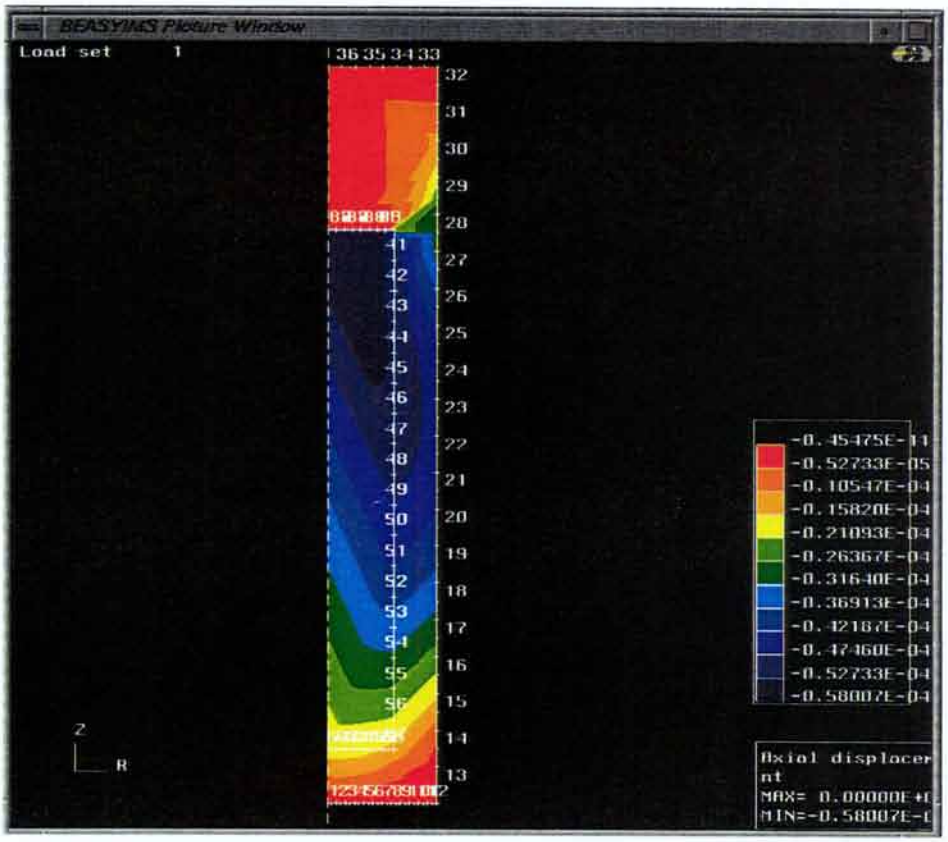
BEASYIMS Picture Window
Load set 1
36 35 34 33
32
31
30
29
28
27
26
25
24
23
22
21
20
19
18
17
16
15
14
13
-0.45475E-11
-0.52733E-05
-0.10547E-04
-0.15820E-04
-0.21093E-04
-0.26367E-04
-0.31640E-04
-0.36913E-04
-0.42187E-04
-0.47460E-04
-0.52733E-04
-0.58007E-04
Z
R
Axial displacer
nt
MAX= 0.00000E+0
MIN=-0.58007E-0

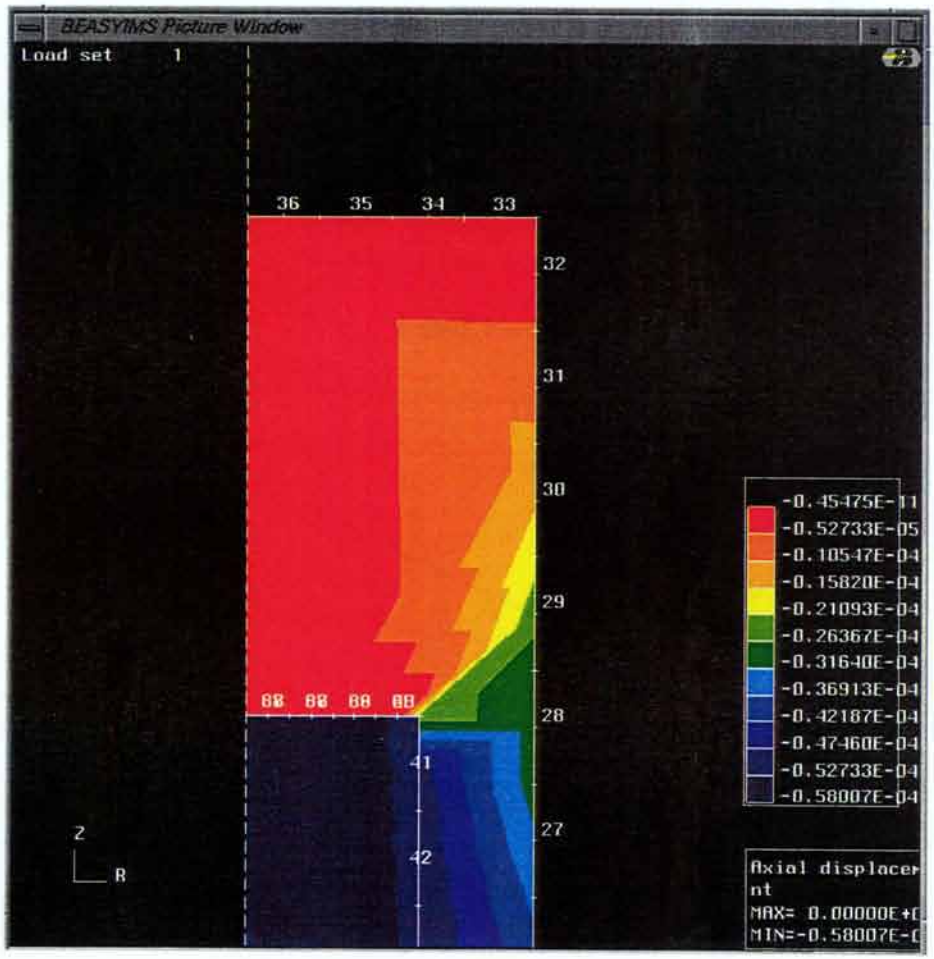
BEASYIMS Picture Window
Load set 1
36 35 34 33
32
31
30
29
28
27
41
42
-0.45475E-11
-0.52733E-05
-0.10547E-04
-0.15820E-04
-0.21093E-04
-0.26367E-04
-0.31640E-04
-0.36913E-04
-0.42187E-04
-0.47460E-04
-0.52733E-04
-0.58007E-04
Z
R
Axial displacer
nt
MAX= 0.00000E+0
MIN=-0.58007E-0

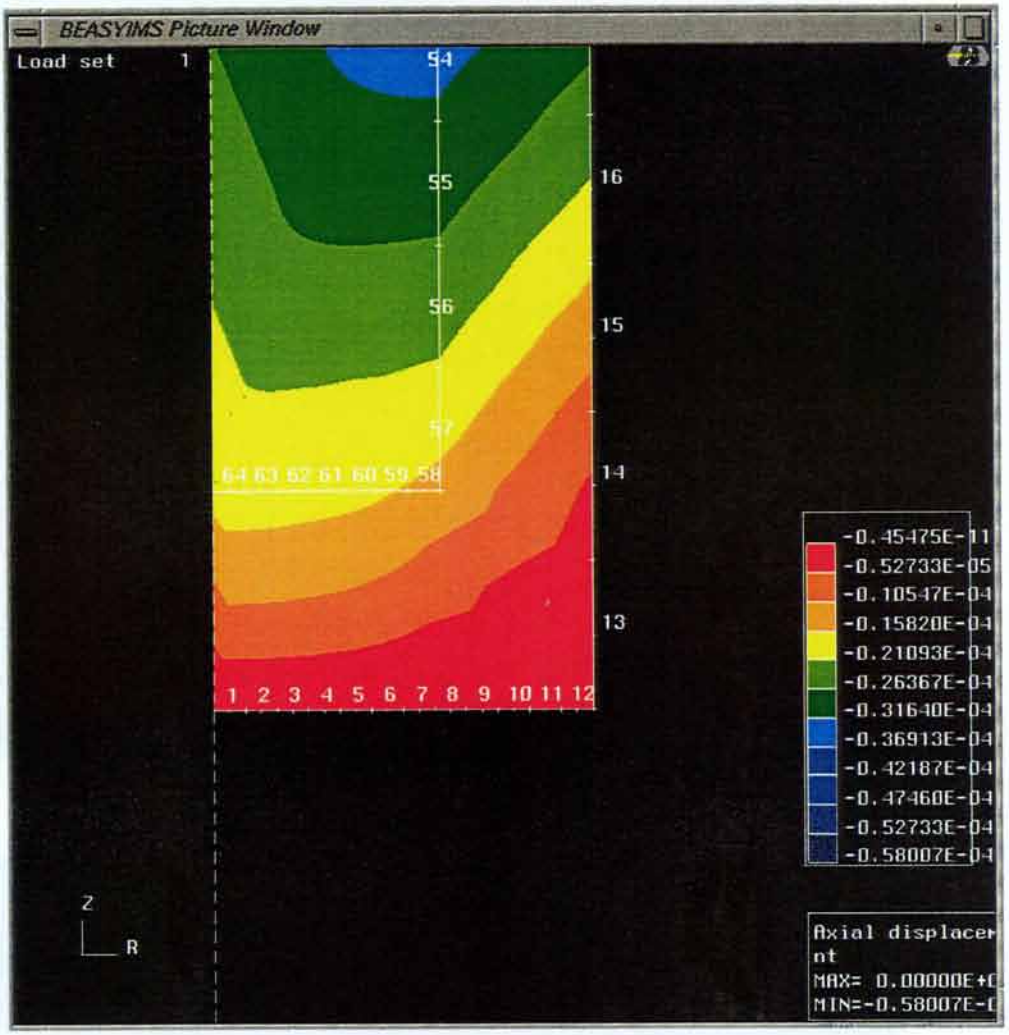
BEASYIMS Picture Window
Load set 1
54
55
56
57
64 63 62 61 60 59 58
16
15
14
13
1 2 3 4 5 6 7 8 9 10 11 12
-0.45475E-11
-0.52733E-05
-0.10547E-04
-0.15820E-04
-0.21093E-04
-0.26367E-04
-0.31640E-04
-0.36913E-04
-0.42187E-04
-0.47460E-04
-0.52733E-04
-0.58007E-04
Z
R
Axial displacement
MAX= 0.00000E+0
MIN=-0.58007E-0


BEASYIMS Picture Window
Load set 1 Symbolic result display
Z
R
Resultant disp't m'tude
: Max result value= 0.58007E-04


BEASYIMS Picture Window
Load set 1 Symbolic result display
Z
R
Resultant disp't m'tude
: Max result value= 0.58007E-04


BEASYIMS Picture Window
Load set 1 Symbolic result display
Z
R
Resultant disp't m'tude
: Max result value= 0.58007E-04

CASE II.

No slip case. The upper of the clay end was assumed to be open.
It was taken two zones with the following properties:

- Zone 1= Lines 1, 2, 3, 4, 5, 6
- *Body forces.-*
  Acceleration 0.0000000E+00 -9.8100004E+00 0.0000000E+00 (m/s^2)
- *Zone properties.-*
  Youngs Modulus 3.0000000E+08 Pa.
  Poissons Ratio 4.9000001E-01
  Density 2.0500000E+03 (kg/m^3)
- *Boundary conditions.-*
  Normal displacement = 0 → lines 1, 2, 3.

- Zone 2= Lines 15, 5 ,6
- *Body forces.-*
  Acceleration 0.0000000E+00 -9.8100004E+00 0.0000000E+00 (m/s^2)
- *Zone properties.-*
  Youngs Modulus 3.0000000E+09 Pa.
  Poissons Ratio 3.0000001E-01
  Density 4.8119409E+03 (kg/m^3)

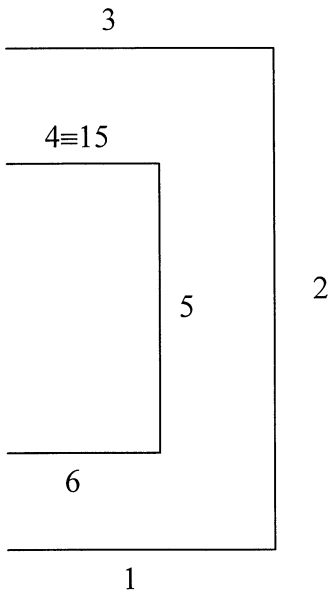

- Resolving $\int_v Ddv = \sum_1^{56} D_i v_i$, where $D= \sigma_1 - \sigma_2$ for each internal point.

Internal Point	σ1(Pa)	σ2(Pa)	D(Pa)	v(m^3)	D(Pa) x v(m^3)
1	-105050	-108150	3100	0.000966	2.9958
2	-104460	-110250	5790	0.000966	5.5955
3	-104120	-112180	8060	0.000966	7.7892
4	-104130	-113880	9750	0.000966	9.4224
5	-104520	-115410	10890	0.000966	10.5241
6	-105270	-116840	11570	0.000966	11.1812
7	-106350	-118250	11900	0.000966	11.5002
8	-105020	-108210	3190	0.002899	9.2484
9	-104400	-110260	5860	0.002899	16.9893
10	-104040	-112140	8100	0.002899	23.4835
11	-104050	-113800	9750	0.002899	28.2672
12	-104440	-115280	10840	0.002899	31.4273
13	-105200	-116670	11470	0.002899	33.2538
14	-106280	-118050	11770	0.002899	34.1236
15	-104980	-108330	3350	0.004832	16.1872
16	-104290	-110280	5990	0.004832	28.9437
17	-103890	-112070	8180	0.004832	39.5258
18	-103880	-113620	9740	0.004832	47.0637
19	-104290	-114990	10700	0.004832	51.7024
20	-105070	-116300	11230	0.004832	54.2634
21	-106160	-117650	11490	0.004832	55.5197
22	-104920	-108520	3600	0.006765	24.3533
23	-104110	-110330	6220	0.006765	42.0771
24	-103630	-111950	8320	0.006765	56.2831
25	-103620	-113310	9690	0.006765	65.5509
26	-104060	-114530	10470	0.006765	70.8275
27	-104870	-115730	10860	0.006765	73.4657
28	-105990	-117030	11040	0.006765	74.6834
29	-104850	-108830	3980	0.008698	34.6165
30	-103820	-110420	6600	0.008698	57.4042
31	-103250	-111750	8500	0.008698	73.9296
32	-103250	-112830	9580	0.008698	83.3230
33	-103750	-113840	10090	0.008698	87.7588
34	-104620	-114920	10300	0.008698	89.5853
35	-105760	-116150	10390	0.008698	90.3681
36	-104800	-109370	4570	0.01063	48.5809
37	-103350	-110530	7180	0.01063	76.3263
38	-102670	-111360	8690	0.01063	92.3782
39	-102750	-112080	9330	0.01063	99.1816
40	-103360	-112880	9520	0.01063	101.2014
41	-104320	-113840	9520	0.01063	101.2014
42	-105510	-115020	9510	0.01063	101.0951

Internal Point	σ1(Pa)	σ2(Pa)	D(Pa)	v(m^3)	D(Pa) x v(m^3)
43	-104730	-110400	5670	0.012563	71.2334
44	-102480	-110440	7960	0.012563	100.0031
45	-101830	-110540	8710	0.012563	109.4255
46	-102130	-110950	8820	0.012563	110.8074
47	-102930	-111610	8680	0.012563	109.0486
48	-104000	-112510	8510	0.012563	106.9129
49	-105250	-113660	8410	0.012563	105.6565
50	-103660	-111990	8330	0.014496	120.7517
51	-100750	-109100	8350	0.014496	121.0416
52	-100700	-108930	8230	0.014496	119.3021
53	-101420	-109370	7950	0.014496	115.2432
54	-102470	-110070	7600	0.014496	110.1696
55	-103690	-110990	7300	0.014496	105.8208
56	-105010	-112150	7140	0.014496	103.5015

$$\int_v Ddv = \sum_1^{56} D_i v_i = 3582.12 \text{ Kg}\cdot\text{m}^2/\text{s}^2$$

- A= Area of the base of the cylinder = 0.866 m^2.
- t_0= 2500 s
- h= clay below the canister = 0.5 m.
- Volume= 0.433 m^3.

- Average Deviator = $\frac{\sum_1^{56} D_i v_i}{\text{Volume}} = \frac{3582.12}{0.866 \cdot 0.5} = 8272.80$ Pa

- Shear Stress= $\frac{\text{Average Deviator}}{2} = 4136.40$ Pa

- Scaling the experimental and our values for the equation $\gamma = B\ln(t + t_0) + A$.

$$\gamma = \frac{\text{Shear Stress}}{\text{Shear Stress (experimental)}}\left[B\ln(t + t0) + A\right]$$

- The settlement of the canister $\delta = h \times \gamma$

$$\delta = h \cdot \left[\frac{\text{Shear Stress}}{\text{Shear Stress (experimental)}}\left[B\ln(t + t_0) + A\right]\right]$$

$$\delta = 0.5 \cdot \left[\frac{4136.40}{1 \cdot 10^5}\left[2 \cdot 10^{-4} \ln(t + 2500) - 1 \cdot 10^{-3}\right]\right]$$

Calculating this equation for difference times, results in the following table:

t(years)	t(seconds)	Δ_{av}(m)	Δ_{av}(mm)
1	31536000	5.074E-05	0.051
10	315360000	6.026E-05	0.060
100	3.154E+09	6.979E-05	0.070
1000	3.154E+10	7.931E-05	0.079
10000	3.154E+11	8.884E-05	0.089
100000	3.154E+12	9.836E-05	0.098
1000000	3.154E+13	1.079E-04	0.108

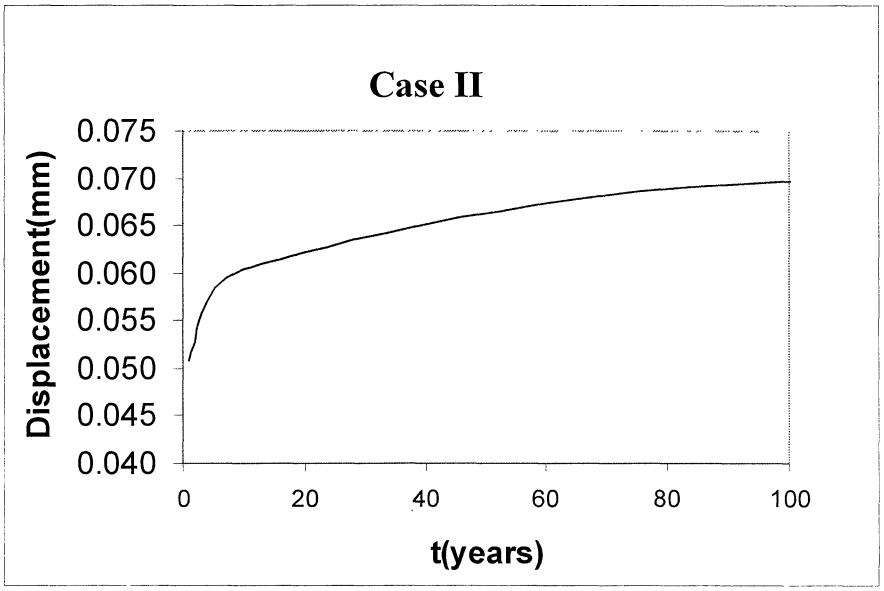

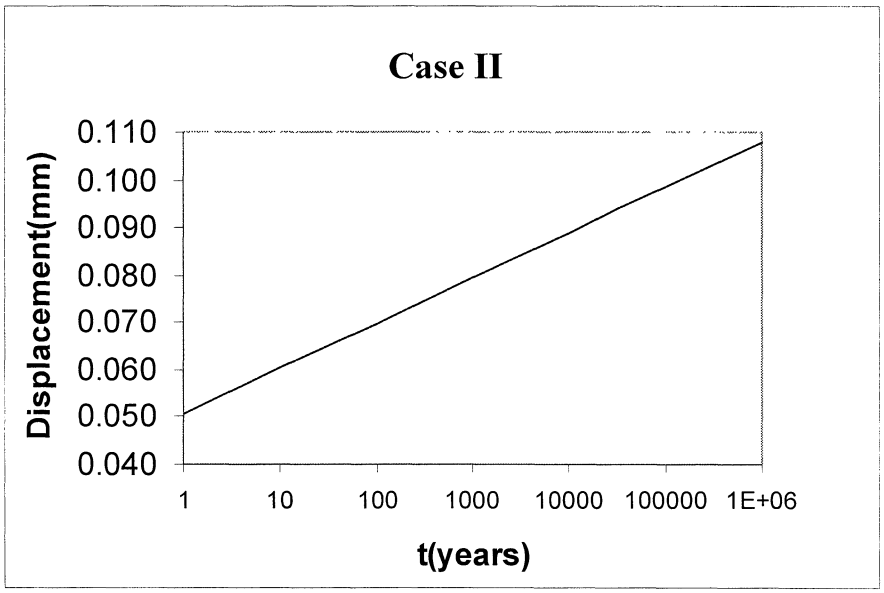

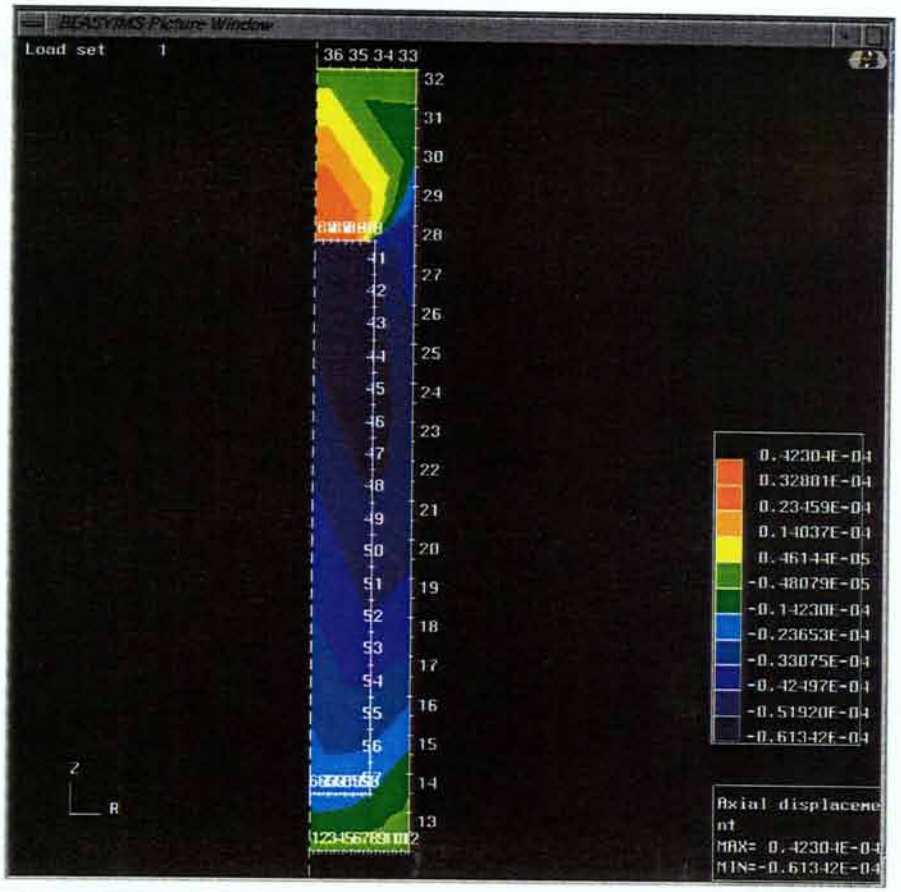
BEASYMS Picture Window
Load set 1
36 35 34 33
32
31
30
29
28
27
26
25
24
23
22
21
20
19
18
17
16
15
14
13
41
42
43
44
45
46
47
48
49
50
51
52
53
54
55
56
0.42304E-04
0.32881E-04
0.23459E-04
0.14037E-04
0.46144E-05
-0.48079E-05
-0.14230E-04
-0.23653E-04
-0.33075E-04
-0.42497E-04
-0.51920E-04
-0.61342E-04
Axial displacement
MAX= 0.42304E-04
MIN=-0.61342E-04
Z
R

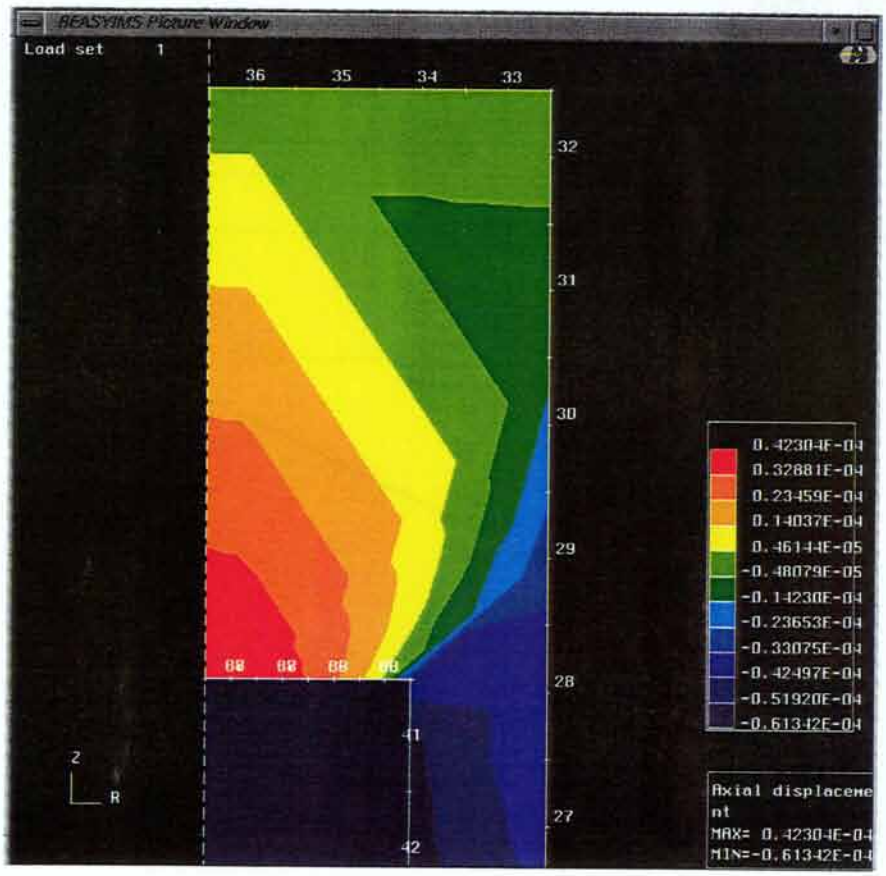
BEASYMS Picture Window
Load set 1
36 35 34 33
32
31
30
29
28
27
41
42
0.42304E-04
0.32881E-04
0.23459E-04
0.14037E-04
0.46144E-05
-0.48079E-05
-0.14230E-04
-0.23653E-04
-0.33075E-04
-0.42497E-04
-0.51920E-04
-0.61342E-04
Axial displacement
MAX= 0.42304E-04
MIN=-0.61342E-04
Z
R

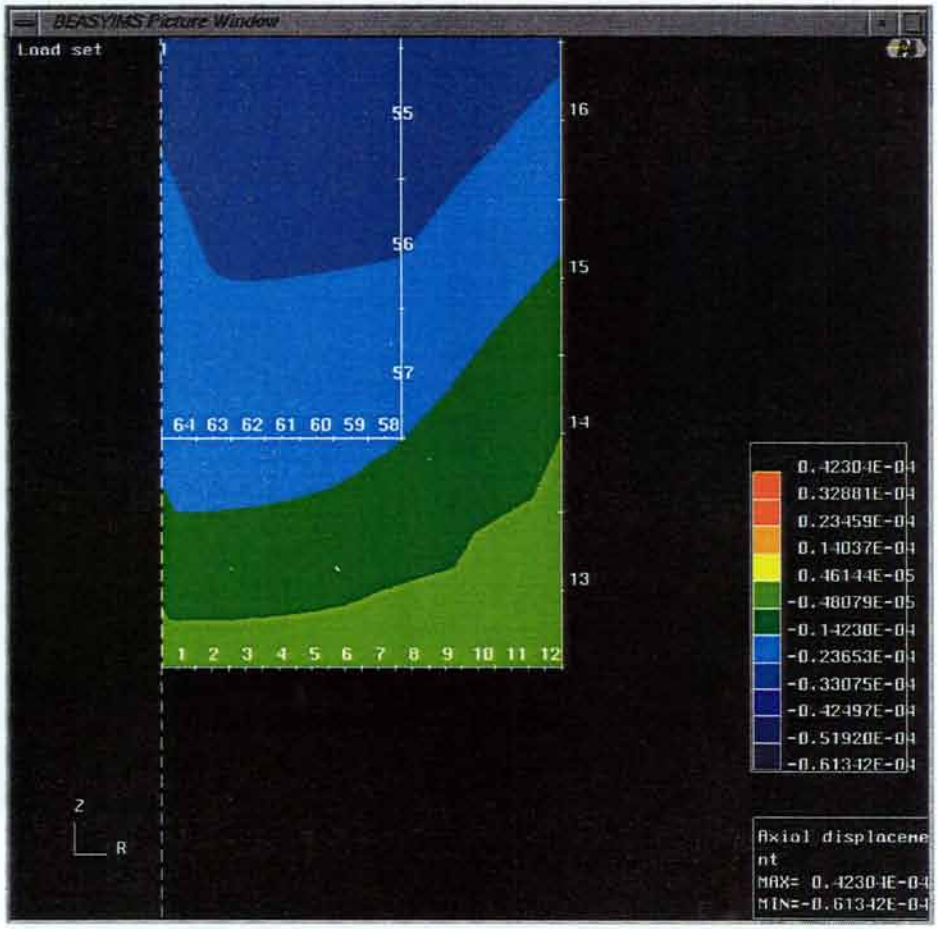
BEASYIMS Picture Window
Load set
55
56
57
64 63 62 61 60 59 58
16
15
14
13
1 2 3 4 5 6 7 8 9 10 11 12
0.42304E-04
0.32881E-04
0.23459E-04
0.14037E-04
0.46144E-05
-0.48079E-05
-0.14230E-04
-0.23653E-04
-0.33075E-04
-0.42497E-04
-0.51920E-04
-0.61342E-04
Z
R
Axial displacement
MAX= 0.42304E-04
MIN=-0.61342E-04

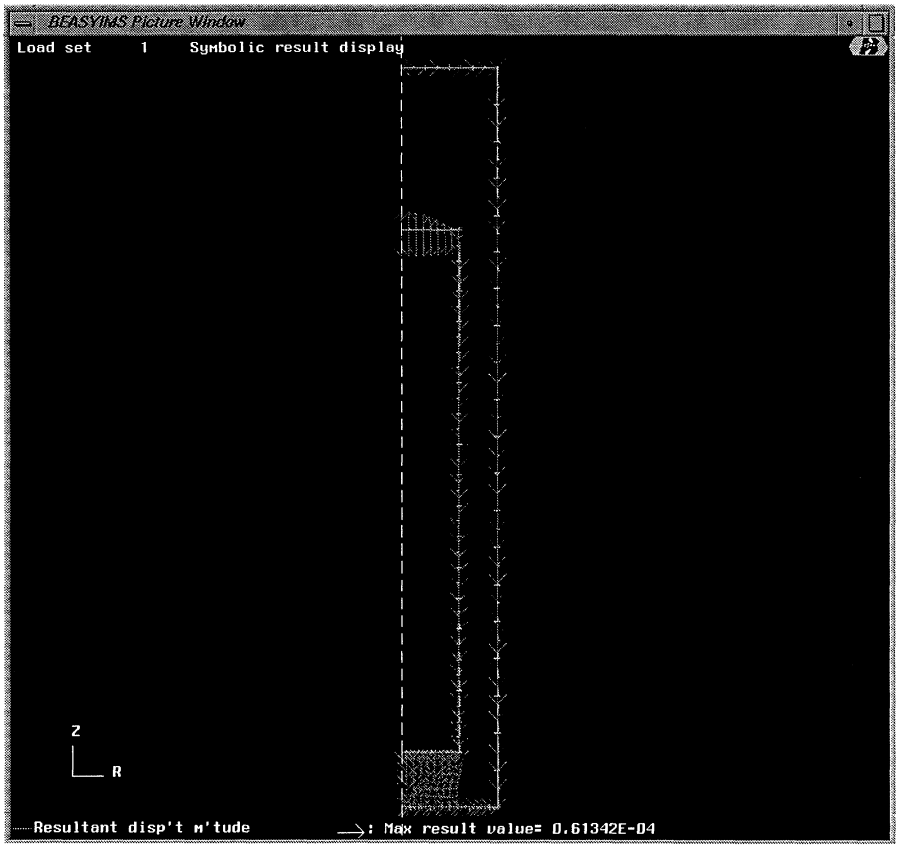
BEASYIMS Picture Window
Load set 1 Symbolic result display
Z
R
Resultant disp't m'tude
: Max result value= 0.61342E-04


BEASYIMS Picture Window
Load set 1 Symbolic result display
Z
R
Resultant disp't m'tude
: Max result value= 0.61342E-04

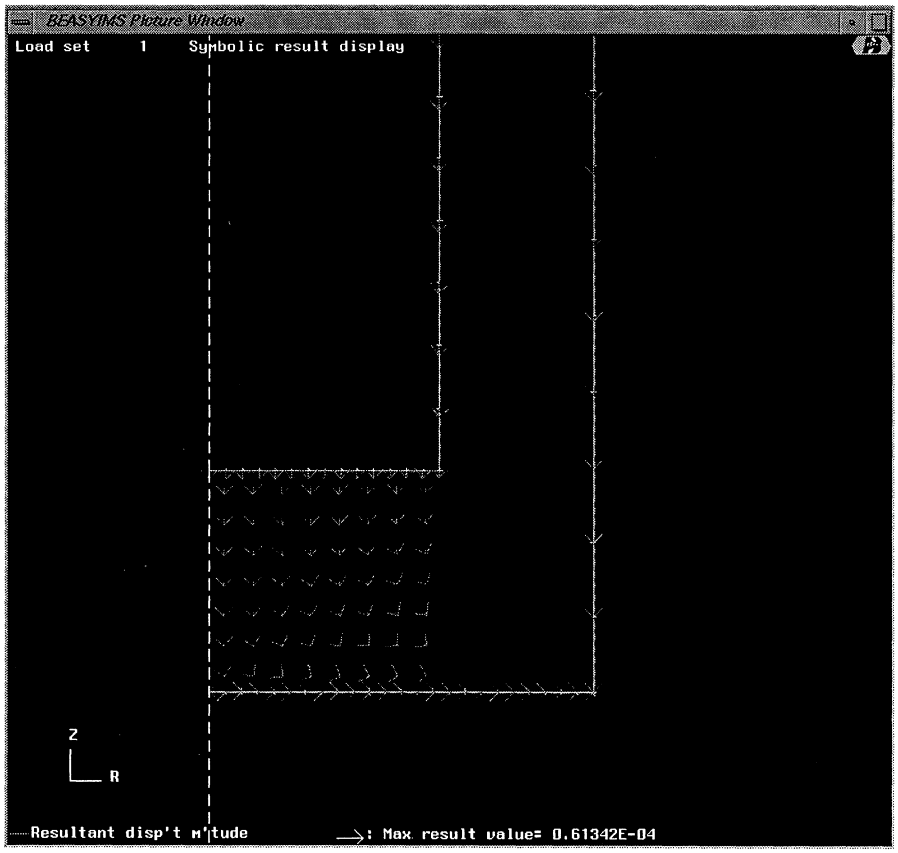
BEASYMS Picture Window
Load set 1 Symbolic result display
Z
R
Resultant disp't m'tude
: Max result value= 0.61342E-04

ISSN 1404-0344
CM Gruppen AB, Bromma, 1999